To the Graduate Council:

I am submitting herewith a thesis written by Wei Jiang entitled "Pulse Measurement for 17-inches KamLAND Photomultiplier Tube." I have examined the final paper copy of this thesis for form and content and recommend that it be accepted in partial fulfillment of the requirements for the degree of Master of Science, with a major in Physics.

Soren P. Sorensen for Yuri Kamyshkov

Yuri Kamyshkov, Major Professor

We have read this thesis
and recommend its acceptance:

William Bugg

Chia C. Shih

Accepted for the Council:

Vice Provost and Dean of Graduate Studies

Thesis
2002
.J535

Pulse Measurement for 17-inches KamLAND Photomultiplier Tube

A Thesis Presented for the Master of Science Degree
The University of Tennessee, Knoxville

Wei Jiang

August 2002

Dedication

This thesis is dedicated to my parents, Huang Qing Chiang and Lan Sheng Zhu, who have always supported me in my whole life and given me endless encouragement, and to Erika Fuentes, who has given me love and support throughout my graduate studies.

Acknowledgement

First, I would like to thank my thesis advisor, Dr. Yuri Kamyshkov for his guidance, advice and support throughout the research. Also, I would like to thank other members of my committee: Dr. William Bugg and Dr. Chia C. Shih for their help and advices. Specially, I would like to express appreciation to Dr. Yuri Efremenko for his guidance and help in data acquisition and analysis. Furthermore I would like to thank Steve Berridge for his help with my experiment equipment.

Abstract

In order to provide input for the Monte Carlo simulation in KamLAND experiment, we studied the several types of abnormal pulses with a Hamamatsu R7250 17" photomultiplier tube (PMT), which is being used in KamLAND detector. In prepulse measurement, by using different incident light intensities, we measured the secondary emission ratio for first dynode and the dynode efficiency to photons, which can also be used in studying of Single Photoelectron (SPE) spectrum width. In afterpulse measurement we separated two types of afterpulses by using the coincidence of delayed afterpulse signal and normal PMT signal. Both of them will produce single photoelectron signal and the probability of occurrence is 3.5% and 4.5%. In latepulse studies we introduced a multi-hit Time Digital Converter (TDC) to perform the time spectrum measurement. Comparing with Hamamatsu latepulse measurements, we obtained a much more detailed time spectrum and have more accurate background subtraction. The total probability of occurrence for latepulse is measured to be 9%. Our results in amplitude study for latepulses indicate that all the peaks seen in the time spectrum are single photoelectron spectrums.

Table of Contents

List of Figures

Chapter I Introduction

1.1 The Solar Neutrino Problem and Neutrino Oscillation

For more than 30 years, experiments have been trying to detect the neutrinos flux produced in the fusion reactions in the core of the Sun. The results of the experiment have been incompatible with the Stand Solar Model prediction [1]. The first measurement was performed in 1968 and since then several experiments have been carried out, all of them coming out with much less neutrino flux than the theory predicted. The explanation for Solar Neutrino Problem is either the lack of understanding of the Sun or unknown properties of neutrinos. Since the Standard Solar Model is very successful in describing other aspect of the Sun, more attention was drawn to the possibility that neutrino has unusual properties.

The most popular explanation for the lack of solar neutrino flux is the neutrino oscillation: the electron neutrino changes its flavor to another ($\nu_e \rightarrow \nu_x$) on its way to Earth. The neutrino oscillation requires three flavors of neutrino to have different masses, which is contradictory to the Standard Model of particle physics where neutrinos are massless. The discovery of neutrino oscillation will be a breakthrough in modern physics and will provide evidence for new physics beyond Standard Model.

For massive neutrinos, neutrino flavor eigenstates ν_e, ν_m, ν_t are not the same as mass eigenstates ν_1, ν_2, ν_3. Their relation can be expressed by the mixing matrix:

$$|\nu_x\rangle = U_{x\alpha}|\nu_\alpha\rangle$$

where $x=e,\mu,\tau$ and $\alpha=1,2,3$

Then, we can calculate the probability of one flavor neutrino x_1 change to another flavor x_2. For the simplified case when only two neutrinos are involved:

$$U = \begin{pmatrix} \cos\theta & Sin\theta \\ -\sin\theta & \cos\theta \end{pmatrix}$$

The survival probability $P_{\nu_e \rightarrow \nu_x}$ will be given by:

$$P_{\nu_e \rightarrow \nu_x}(l, E; m, \theta) = \sin^2 2\theta \sin^2(\frac{1.27\Delta m^2 l}{E_\nu}) \quad (1.1)$$

where θ is the mixing angle and Δm^2 is the mass square difference between two neutrino flavors. We can see that if neutrino oscillation is confirmed, the neutrino mass cannot be zero as suggested by Standard Model. For the solar neutrino problem, there are several neutrino oscillation solutions: LMA (large mixing angle), SMA (small mixing angle) and LOW (low Δm^2) for oscillations enhanced by matter effects through the Mikheyer-Smirnov-Wolfenstein mechanism and so called vacuum oscillations [2]. Most of the

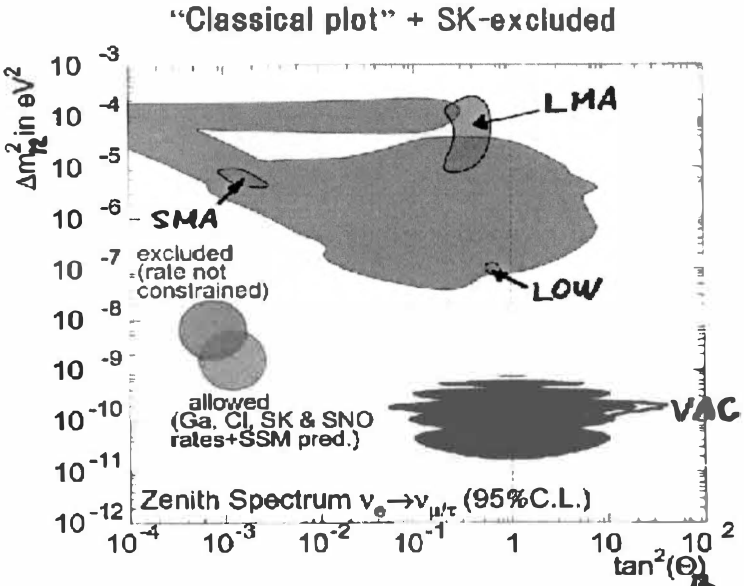

FIGURE 1.1: NEUTRINO OSCILLATION SOLUTIONS [3]

region is already excluded by the recent experimental results (Figure 1.1) [3]. The only solution region left is LMA, which is will be addressed in KamLAND by the measurement of reactor neutrino flux.

1.2 KamLAND Experiment

KamLAND (Kamioka Liquid scintillator Anti-Neutrino Detector) is a large underground anti-neutrino detector built in Japan, whose principle goal is to measure the flux and energy spectrum of anti-neutrinos generated by Japanese commercial nuclear reactors [4]. This experiment will explore the possibility of neutrino oscillation and hence can provide a solution to the solar neutrino puzzle.

KamLAND detects flux of anti-neutrinos from Japanese nuclear reactors located mostly in 150km~200km range. It can detect low energy anti-neutrinos (1.8MeV~10MeV). From the previous discussion, the anti-neutrino oscillation probability:

$$P_{\nu_e \rightarrow \nu_x}(l, E; m, \theta) = \sin^2 2\theta \sin^2\left(\frac{1.27\Delta m^2 l}{E}\right)$$

KamLAND has good sensitivity to Δm^2 since it has a long baseline L and low energy E. It will directly explore the LMA solution of Solar Neutrino Problem. If neutrino oscillation would be confirmed by the experiment, the Standard Model would have to be modified and it would be a fundamental breakthrough in modern physics. If the oscillation is not fund, the LMA solution region will also be excluded and other ideas might be needed to solve the solar neutrino puzzle.

1.3 KamLAND Detector and anti neutrino detection [4]

The scheme of KamLAND detector is shown in Figure 1.2. It consists of 1200m^3 of ultra-pure liquid scintillator, which is surrounded by 2000 m^3 of puffer mineral oil, where 2000 photomultiplier tubes (1325 17" PMT and 554 20" PMT) are immersed. The 17" Hamamatsu R7250 photomultiplier tubes are specially developed for KamLAND experiment, while 20" photomultiplier tubes are taken from old KAMIOKANDE experiment. The 17" tubes have much better time resolution and amplitude resolution as compared to the 20" tubes.

In KamLAND, the anti-neutrino is detected by inverse β decay:

$$\overline{\nu_e} + p \rightarrow n + e^+$$

The positron will deposit the energy and then annihilate with an electron producing two gamma rays (511 keV each). The neutron will be thermalized and then captured by a proton producing a 2.2 MeV gamma ray:

$$n + p \rightarrow d + \gamma$$

Thus, an anti-neutrino event will have a clear signature of an instant positron signal and a delayed 2.2MeV gamma ray signal (Figure 1.3). Since the anti-neutrino detection is using the coincidence of two signals, the background can be suppressed dramatically. The estimated anti-neutrino event rate is 2 events/day while the background is only around 0.1 event/day.

The precision of the measurement depends on how well we will understand the detector and the data. In order to have accurate data analysis we need to simulate the behavior of the detector. For accurate simulation of the R7250 17" photomultiplier tubes we are using in KamLAND experiment, we have measured the response of a 17" photomultiplier tube

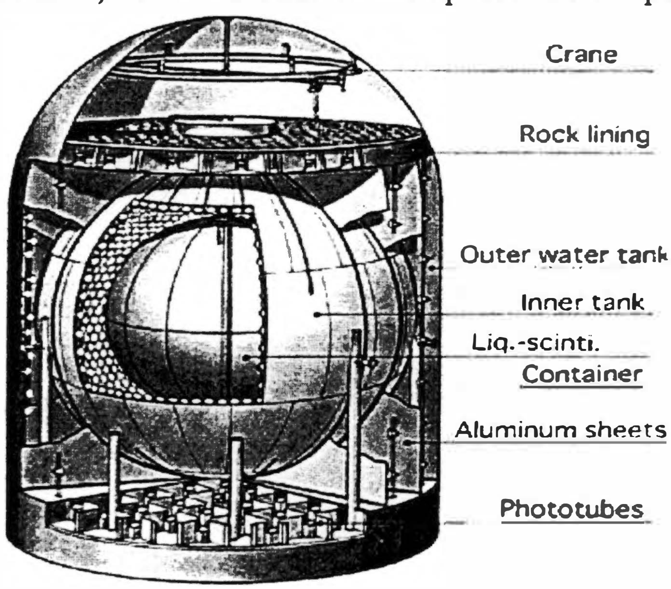

FIGURE 1.2: KAMLAND DETECTOR [4]

to single photoelectron and several types of abnormal pulses in a Hamamatsu R7250 PMT.

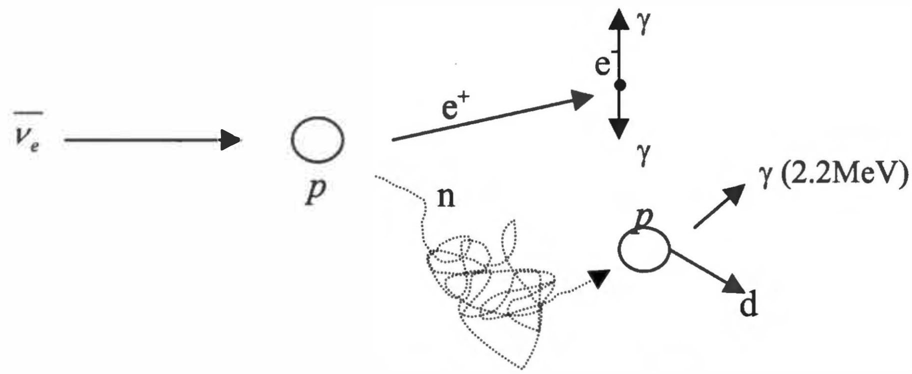

FIGURE 1.3: ANTI-NEUTRINO DETECTION PROCESS

Chapter II Photomultiplier Tube

2.1 Construction Structure [6]

A photomultiplier tube (PMT) (Figure 2.1) consists of several parts: an input window, a photocathode, focusing electrodes, dynode system (electron multiplier) and anode in a vacuum tube. When photons enter the tube, first they will hit the photocathode, and the cathode will emit one or more photoelectrons to vacuum by photoelectric effect. Due to the nature of the effect, the number of photoelectrons emitted by cathode is proportional to the intensity of light. Because of the potential between the photocathode and dynode, the photoelectrons will be pulled towards the dynode and produce a number of secondary electrons. The secondary electrons will be collected and amplified by the dynode system; in the final stage, the electrons will be collected by the anode and produce an output current pulse. Next, we will discuss in detail each of the PMT parts mentioned above:

- Photocathode

The photocathode is a layer of photo-emissive surface consisting of alkali metal with very low work function; it converts the incident photons flux into photoelectrons by external photoelectric effect. The conversion efficiency varies with the wavelength of incident light. The material used in Hamamatsu R7250 is Bialkali (Sb-K-Cs), which consist of two types of alkali metals. Bialkali photocathodes are sensitive to the wavelength from ultra-violet to blue range and they match the spectrum of the scintillator used in KamLAND. The photocathode in R7250 covers a 17" diameter area of the tube front surface.

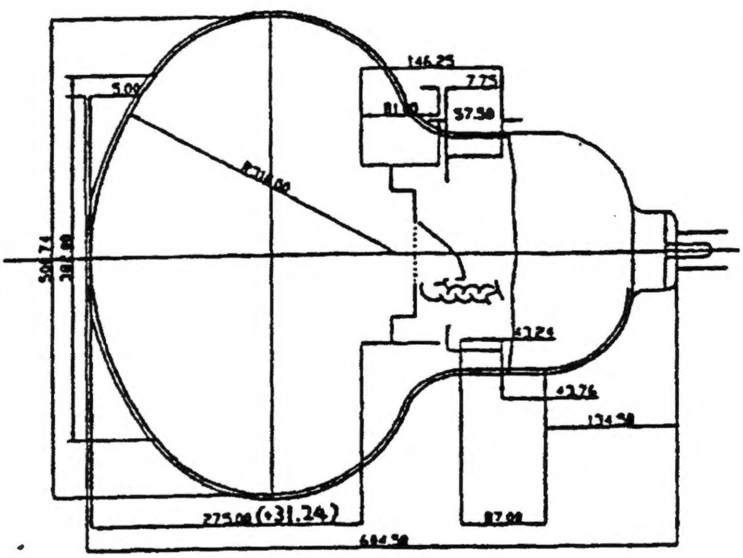

FIGURE 2.1: HAMAMATSU R7250 17" PMT [5]

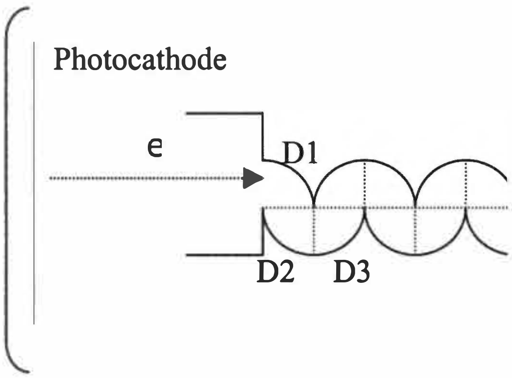

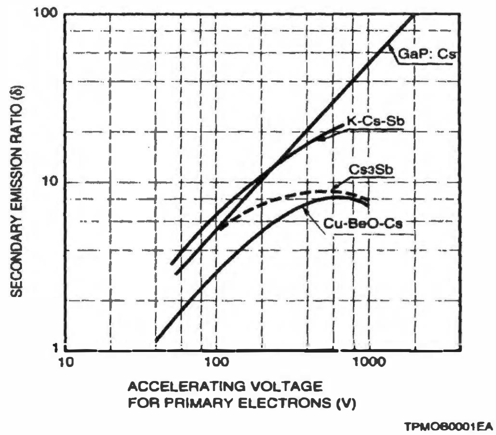

FIGURE 2.2: BOX AND GRID DYNODE SYSTEM FIGURE 2.3: SECONDARY EMISSION RATIO [6]

- Dynode System (Electron Multiplier)

The dynode system type used in R7250 is "box-and-grid". Figure 2.2 is an example of typical box-and-grid type dynode system:

The box-and-grid dynode system has a good collection efficiency and good time resolution. There are totally 10 dynode stages in the Hamamatsu R7250 and the overall gain for its electron multiplier at operating voltage ~2000V is around 10^7.

In Figure 2.3, the secondary electron emission ratios are plotted for several types of dynode. In our measurements, the operating voltage between the photocathode and first dynode is around 815V and the gain at the first dynode is 17 (which will be discussed in Chapter IV).

- Voltage Divider Circuit

The interstage voltages for PMT dynodes are controlled by a voltage divider circuit, which consists of a chain of resistors. The scheme for our voltage divider circuit is shown in Figure 2.4. The total power supply voltage is 1960V (corresponding to the gain of 10^7), which is fixed in all our measurements; we can calculate the voltage between the photocathode and the first dynode:

$$V_d = V_{total} \times \frac{R_1}{\sum_{i=1}^{13} R_i} = 815.5(V)$$

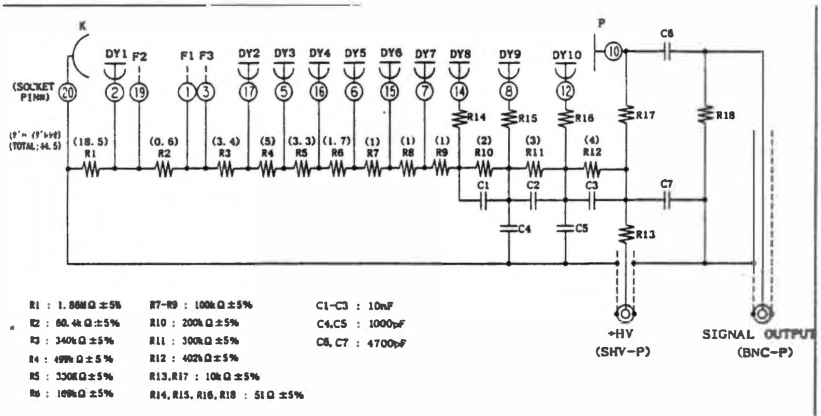

FIGURE 2.4: VOLTAGE DIVIDER CIRCUIT [7]

2.2 Photomultiplier Tube Characteristics

2.2.1 Photocathode Quantum Efficiency

Quantum Efficiency is defined as the ratio of the number of photoelectrons emitted from the photocathode to the number of the incident photons at a given wavelength:

$$Q.E. = \frac{Number\ of\ Phototelectrons}{Number\ of\ Photons} \times 100\%$$

The Quantum Efficiency of R7250 is shown in Figure 2.5.

2.2.2 Gain

Photoelectrons emitted from a photocathode are accelerated by an electric field and gain energy around 815eV; they strike the first dynode and produce secondary electron emissions, which will be collected by next dynode to produce additional secondary electron emissions. By repeating this process over successive dynodes stage (cascade process), it is possible to achieve a high gain [6].

Gain can be defined as the ratio of the number of electrons that are collected by the anode to the number of input photoelectrons, the overall gain for R7250 is around 10^7 while operating at the voltage ~2kV (1960V in our measurements).

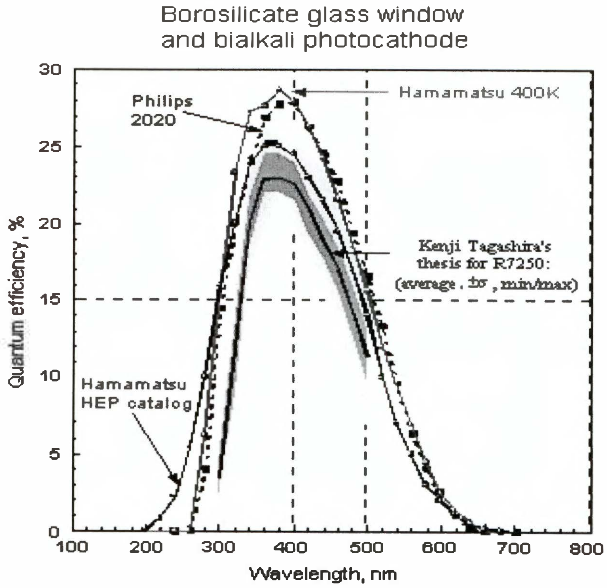

FIGURE 2.5: QUANTUM EFFICIENCY FOR HAMAMATSU R7250 [5]

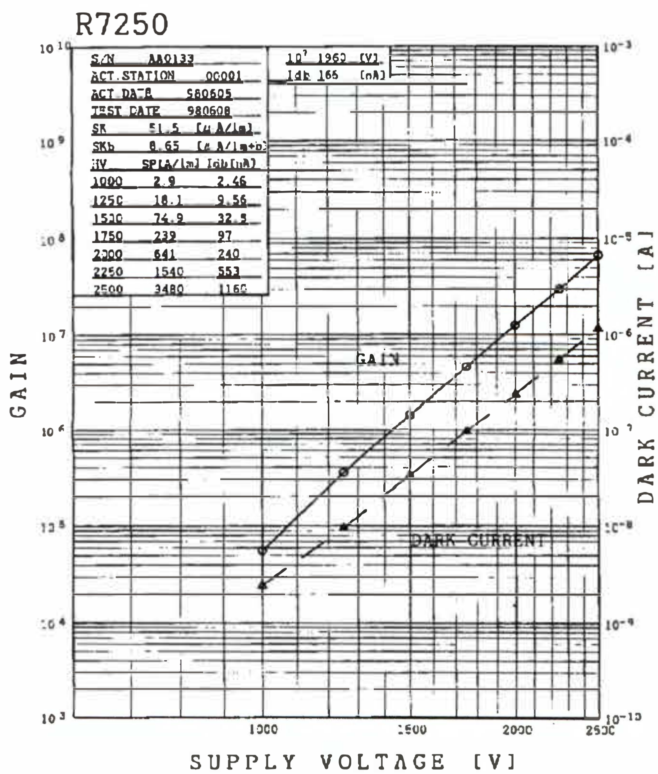

FIGURE 2.6: R7250 GAIN VS SUPPLY VOLTAGE [7]

If η is the average secondary emission ratio, E=βV is the interstage voltage where V is the total operating voltage and β is a constant determined by the voltage divider, we have:

$$\eta = A \cdot E^{\alpha} = A(\beta V)^{\alpha}$$

Here A is constant, and α, which usually has a value of 0.7~0.8, is a coefficient determined by the dynode material. If the electron multiplier has n stages, the total gain G will be:

$$G = \eta_1 \cdot \eta_2 \cdots = A^n \cdot (\prod_{i=1}^{n} \beta_i^{\alpha})(V^{\alpha})^n \propto V^{\alpha n}$$

In our R7250 tube n=10, the gain is extremely sensitive to the power supply voltage. From Figure 2.6 we can see that for operating voltage around 2000V, a 200V difference in voltage will result a factor of two in overall gain of the tube. In our measurement we are using ORTEC 456 high voltage supply for R7250, the voltage is fixed at 1960V and the fluctuation is expected to be less than 1V.

2.2.3 Dark Current

A small amount of photoelectrons are produced in a photomultiplier tube even when it is operated in a complete darkness; this is called dark current and should be minimized in the PMT. The dark current rate in our experiment is measured to be around 30 KHz.

Dark current can have its origin in several processes. The main origin of dark current is the thermionic emission of electrons: since the material of photocathode (or dynode) has a very low work function, it will emit thermionic electrons even at room temperature [6]. These electrons will be amplified by the electron multiplier and give a detectable signal.

Besides the thermionic emission, the other origins of dark current include cosmic rays, glass scintillation and field emission, etc [6]. We should notice that dark current rate also depends on the operating voltage (Figure 2.6) and in order to have an accurate measurement we should keep the dark current as low as possible during our measurements.

Chapter III PMT Response to Single Photoelectron

PMT response to single photoelectron (SPE) is an important property of the tube. It is measured under the condition that the incident light level is so small that only single photoelectron will be produced at the photocathode. For a higher light intensity level, the output signal is simply the overlap of several SPE.

In this section, the measurement of Single Photoelectron is described. The transit time spread and pulse height spectrums are measured. A multiple Gaussian functions distributed by Poisson is introduced as the fitting function to describe the charge spectrum of SPE. The SPE pulse height spectrum is obtained after the pedestal subtraction.

3.1 Experiment Equipment

In our experiment, a 17" Hamamatsu R7250 Photomultiplier Tube is measured under the room temperature. The tube is stored in a black metal test box (Figure 3.1), with all the edges sealed around the front door. A blue LED with wavelength 400nm was used in our experiments as the light source. It is attached to the top of the box. A NIM electronics system is used to trigger the LED and a CAMAC system, which is connected to a PC, is used for data acquisition.

The DAQ system consists of one LeCroy 2249W twelve channel ADC (Analog Digital Converter), one LeCroy 2228A eight channel TDC (Time Digital Converter) and one LeCroy 4208 eight channel TDC (For latepulse measurement).

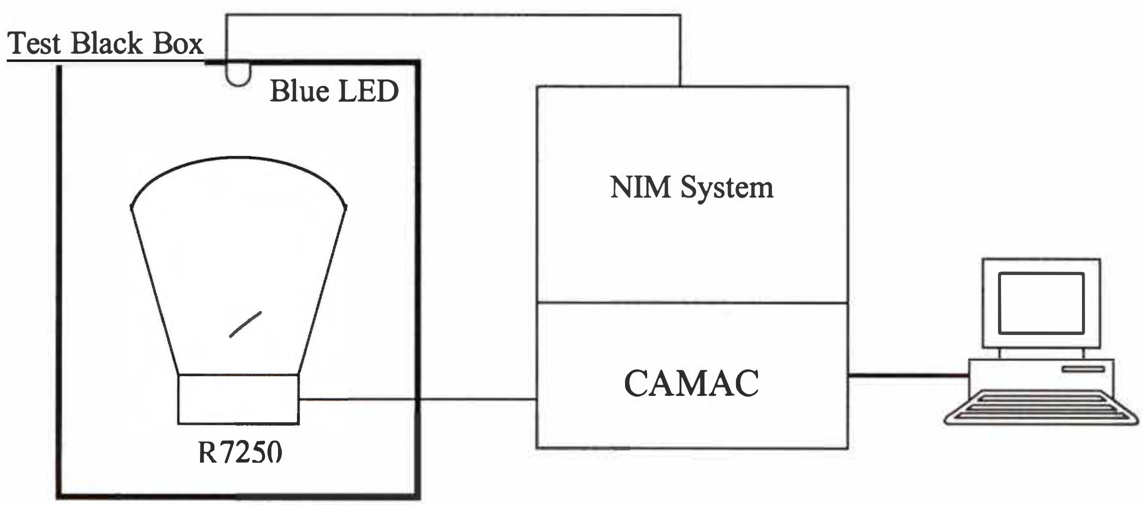

FIGURE 3.1: EXPERIMENT EQUIPMENT

3.2 Experiment Setup

In SPE measurement, the external trigger triggers the LED. Incident light intensity is adjusted to the level that only a single photoelectron is knocked out from the photocathode. The output of PMT is directed into DAQ as shown in Figure 3.2. The timing scheme is shown in Figure 3.3.

3.3 Experimental Results

The measured pulse height distribution is shown in Figure 3.4. We can see that there is a single peak sitting at ~100 channels away from the pedestal. Transit Time Spread is shown in Figure 3.5. The distribution has FWHM=9.3 ns. The transit time spread of PMT, as measured by Hamamatsu, should be better since the total measured transit time spread includes the contribution of LED's width in our case. In KamLAND experiment the TTS is 3~4 ns.

3.4 Discussion

3.4.1 Fitting Function

The number of photoelectrons produced at the photocathode has a Poisson distribution:

$$P(n,\lambda) = \frac{\lambda^n e^{-\lambda}}{n!}$$

where λ is the average number of photoelectrons produced.

Since the electron multiplier has 9 stages with an overall gain of approximately 10^7, according to the center limit theorem, the pulse height distribution for SPE at the output should have Gaussian distribution. The pulse height distribution for double photoelectron should be simple combination of two Gaussian distributions. The mean value and σ^2 will be twice of SPE spectrum.

From the discussion above, we built the fitting function with multiple Gaussian functions distributed in Poisson distribution as follows:

$$\begin{aligned} & f(x; A, \lambda, p_0, \sigma_0, d_1, \sigma_1) \\ &= A\{P(0,\lambda)\Gamma(x; p_0, \sigma_0) + P(1,\lambda)\Gamma(x; p_0 + d, \sigma_1) + P(2,\lambda)\Gamma(x; p_0 + 2d, \sqrt{2}\sigma) + \ldots\} \\ &= A\left\{P(0,\lambda)\Gamma(x; p_0, \sigma_0) + \sum_{n=1}^{20} P(n,\lambda)\Gamma(x; p_0 + nd, \sqrt{n}\sigma_1)\right\} \end{aligned}$$

Here $\Gamma(x;\, p,\sigma)$ is the Gaussian distribution:

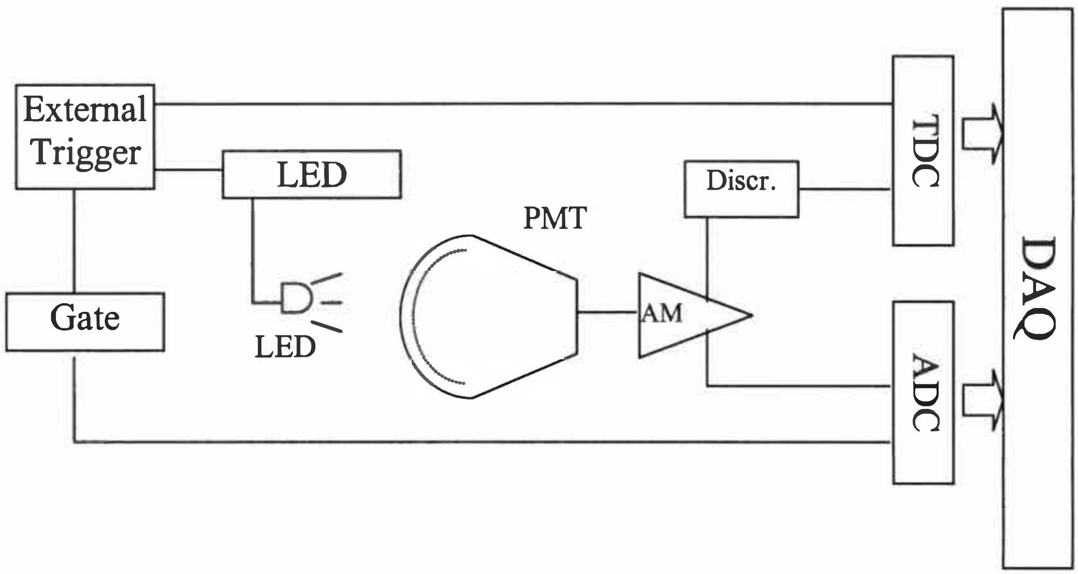

FIGURE 3.2: EXPERIMENT SETUP

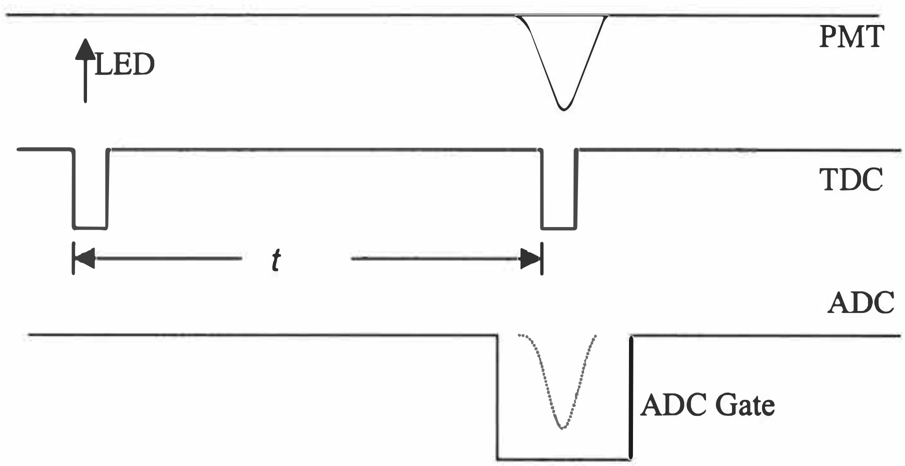

FIGURE 3.3 TIMING SCHEME FOR SPE MEASUREMENT

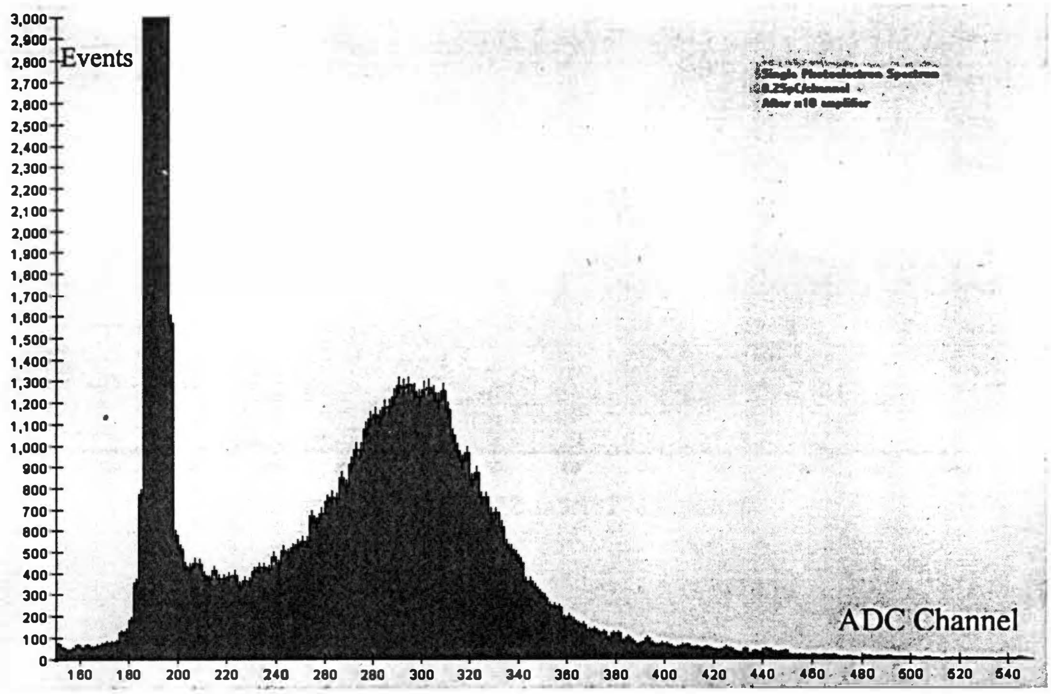

FIGURE 3.4: SPE PULSE HEIGHT DISTRIBUTION

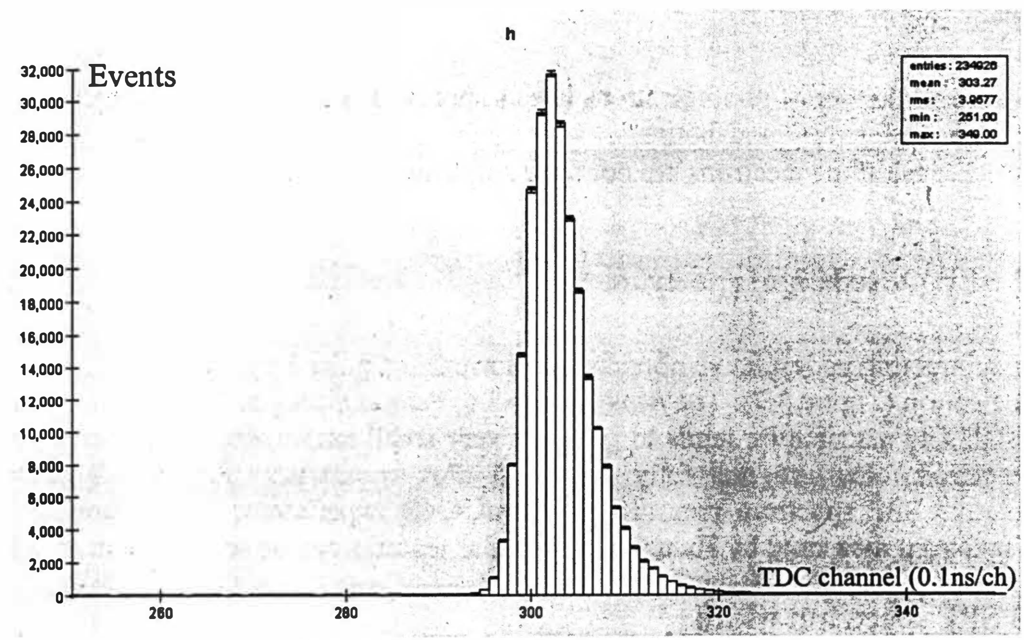

FIGURE 3.5: TRANSITION TIME SPREAD

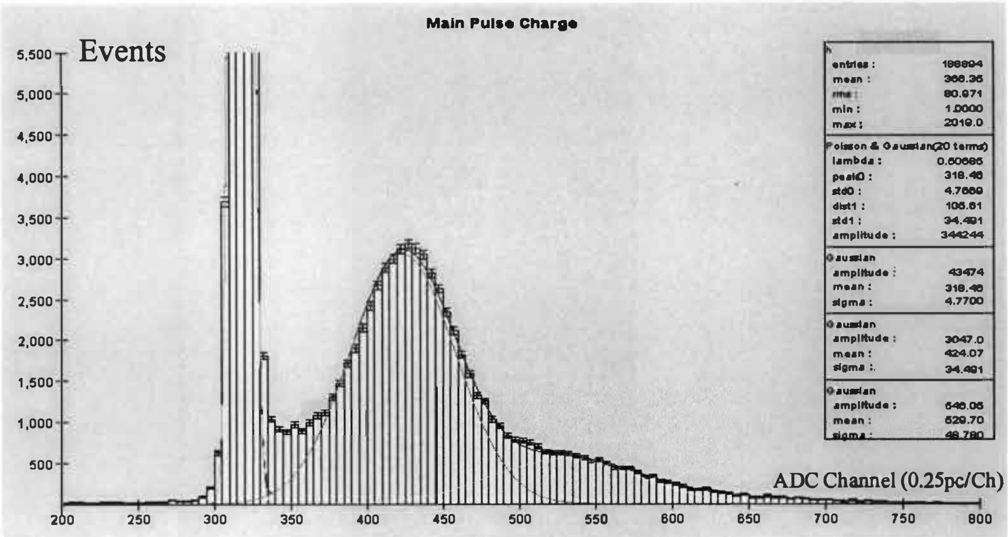

FIGURE 3.6: TYPICAL SPE SPECTRUM FITTING

$$\Gamma(x, p, \sigma) = \frac{1}{\sigma\sqrt{2\pi}} e^{-\frac{(x-p)^2}{2\sigma^2}}$$

p_0 and σ_0 are the position and width of pedestal, d and σ_1 are the mean value and deviation of the first peak. A is the overall amplitude and λ is the average number of photoelectrons produced at the photocathode. Figure 3.6 is a typical fit of a pulse height distribution:

The average number of photoelectrons in this spectrum is 0.51 and we can clearly see the double photoelectron contribution. However, the fitting is not good at lower amplitude region because some electrons are not fully amplified in the electron multiplier.

3.4.2 SPE pulse height spectrum

After subtracting pedestal, we obtained the normalized pulse height distribution for single photoelectron (Figure 3.7): The peak/valley=3.6, Peak is sitting at 102 channels above the pedestal. The distribution tends to go up at very small amplitude, which corresponds to the electrons that are not fully amplified. For comparison Figure 3.8 shows the cumulative SPE spectrum measured in KamLAND experiment; and Figure 3.9 shows SPE spectrum measured by Hamamatsu. Similar features can be seen in them as well.

3.4.3 SPE spectrum width

The width of SPE spectrum is due to the overall fluctuation of the PMT. Several factors' fluctuation contributes to the final width: the number of dynode electrons at the 1st dynode, the amplification factor of the electron multiplier after the first dynode and non-uniformity of the collection efficiency, etc. We measured the gain at the first dynode (§ 4.4) and the fluctuation of the electron multiplier (§ 4.3):

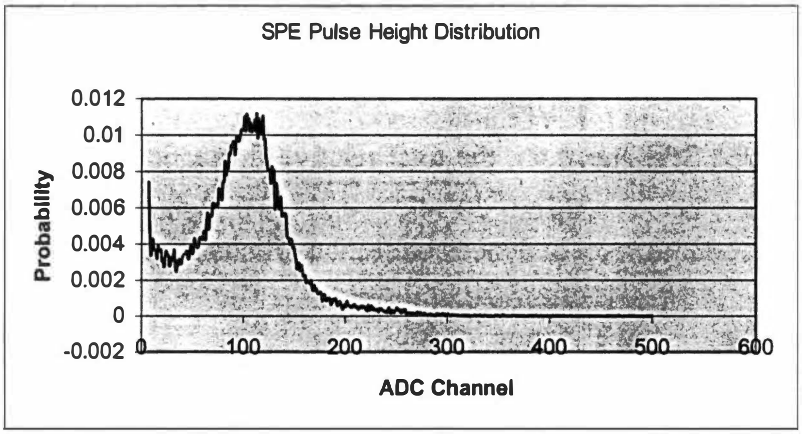

FIGURE 3.7: SPE PULSE HEIGHT DISTRIBUTION (PEDESTAL SUBTRACTED)

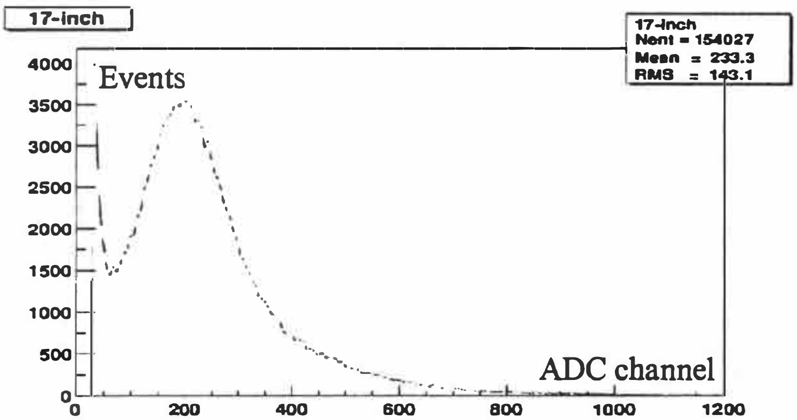

FIGURE 3.8: CUMULATIVE SPE SPECTRUM IN KAMLAND

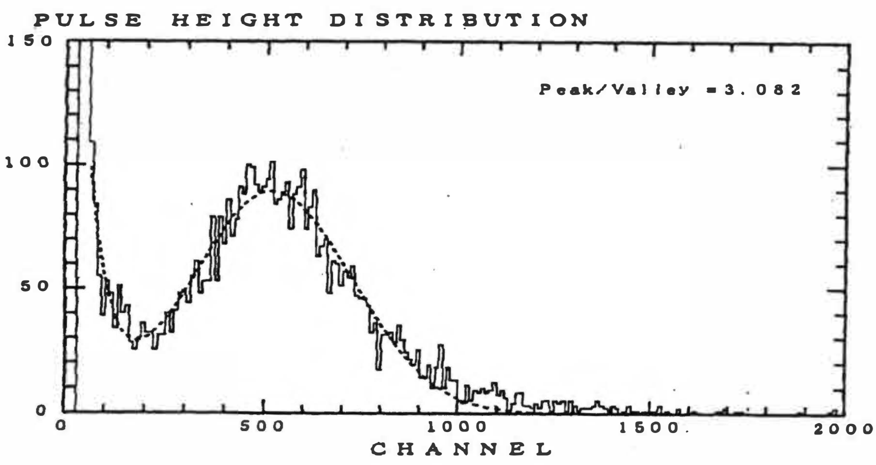

FIGURE 3.9: SPE SPECTRUM MEASURED BY HAMAMATSU[7]

The gain at first dynode is measured to be 17. Then, the relative Poisson variation will be $17^{-1/2} = 0.243$. For the electron multiplier after the first dynode, the mean position is 5.95 channel and the fluctuation is 3.03 channel (see § 4.3 and § 4.4). Thus, total relative fluctuation due to multiplication of the first dynode and the electron multiplier is:

$$\sqrt{\left(\frac{1}{\sqrt{17}}\right)^2 + \left(\frac{3.03/5.95}{\sqrt{17}}\right)^2} = 0.27$$

From the measured SPE spectrum, the total relative fluctuation is ~ (35/102) = 0.343. Then the difference between them: $\sqrt{0.343^2 - 0.27^2} = 0.2$ should be attributed to other factors such as non-uniformity of dynode collection efficiency, etc.

Chapter IV Prepulse Measurements

When photons enter the photomultiplier tube, some of them pass through the photocathode without producing any photoelectrons and directly hit the first dynode. These photons might knock out one or more electrons (Dynode Electrons), which will be colleted by the second dynode and amplified by the electron multiplier, thus give a signal prior to the main pulse (Figure 4.1). Such kind of signal, so called "prepulse", is relatively small compared to the normal signal since it does not have amplification of the first dynode. The prepulse is prior to main signal since the photon will cross the vacuum between phαtocathode and dynode at the speed of light while the photo-electron have a drifting time around 55 ns for R7250. The probability of occurrence will depend on the quantum efficiency of first dynode.

In this section the techniques for measuring the prepulse parameters are described. The measurements are made with different incident light intensities. The results are fitted with the same function as the one we used for SPE measurement since they are basically produced by the same mechanism. By comparing the fitted amplitude spectrum we calculated that the gain at the first dynode for photoelectron is around 17 and the dynode efficiency to LED photons is 2.9%.

4.1 Quantum Efficiency of 1st Dynode

Suppose there are N photons coming to the photomultiplier tube and the Quantum Efficiency of the photocathode is ξ (We assumed ~22%, see Figure 2.5); there will be ξN photoelectrons produced at the photocathode and $(1-\xi)N$ photons will pass through the photothode. If all of them hit the 1st dynode and the quantum efficiency of 1st dynode is η, there will be $\eta(1-\xi)N$ Dynode Electrons knocked out from the dynode. If the gain at

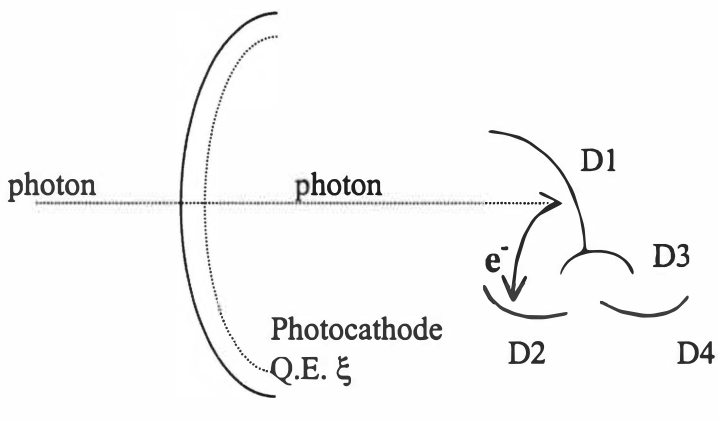

FIGURE 4.1: PREPULSE MECHANISM

the first dynode for photoelectrons is G_1, the ξN photoelectrons will produce $\xi G_1 N$ Dynode Electrons. The ratio between normal signal pulse (produced by photoelectrons) and prepulse (produced by photons) will be:

$$r = \xi G_1 N / \eta(1-\xi)N = \xi G_1 / \eta(1-\xi) \qquad (4.1)$$

In prepulse measurement we evaluate the amplitude for both main signal and prepulse signal. By comparing the amplitude spectrum of normal signal and prepulse signal we calculate the gain G_1 at 1^{st} dynode and the dynode efficiency for photons. Then, from formula (4.1) one can find the Quantum Efficiency of the dynode.

4.2 Experiment Setup

Since the prepulse is caused by photons hitting dynode, the direction of incident light is a critical factor that has to be under control. In this measurement we introduced a thin light pointing tube in front of the LED, by pointing the tube to the right direction we can control whether the light illuminates 1^{st} dynode or not. The experiment setup is shown in Figure 4.2.

By carefully selecting the delay after the amplifier we can catch both prepulse signal and normal signal with the same ADC time gate. The timing scheme is shown in Figure 4.3.

The ADC gate is chosen to be 60ns and threshold is set at 0.4mV of PMT signal. As described above, we measured the prepulse with several incident light intensities: ~55 P.E., 16 P.E. and SPE level.

4.3 Experimental Results

4.3.1 Light aiming at dynode & off dynode

With large incident light intensity (~ 55 P.E.), the prepulse happens 100% time. When we move the light pointing tube off the dynode, the prepulse disappears from the oscilloscope (See Figure 4.4).

4.3.2 Prepulse Timing Properties:

The time distribution for prepulse compared to the main pulse is shown in Figure 4.5. The prepulse signal occurs at around τ = 60 ns prior to the main signal, this value is the flight time for an electron drifting from the photocathode to the dynode, taking into account the rise-time effect in discriminator.

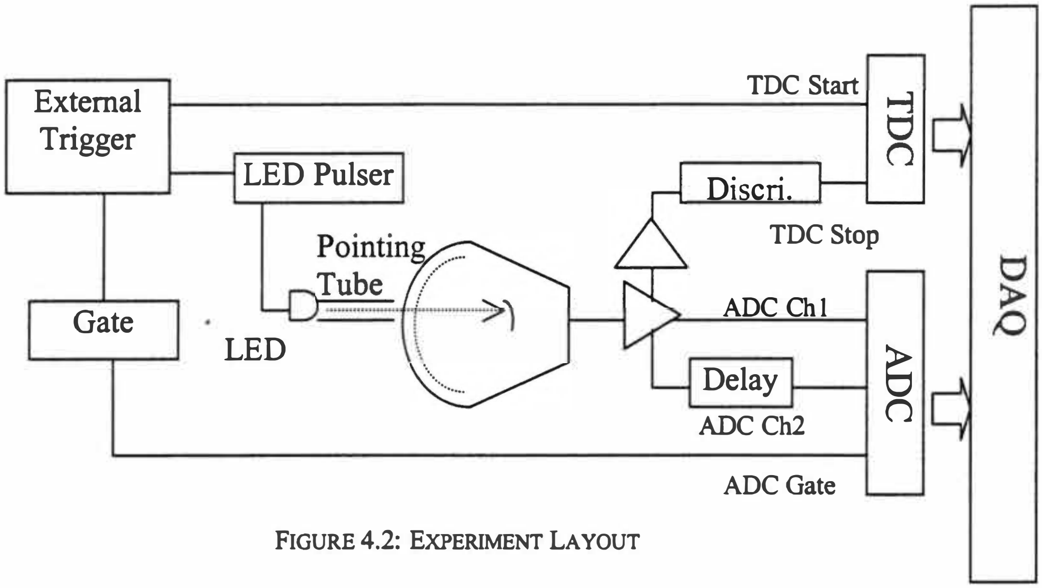

FIGURE 4.2: EXPERIMENT LAYOUT

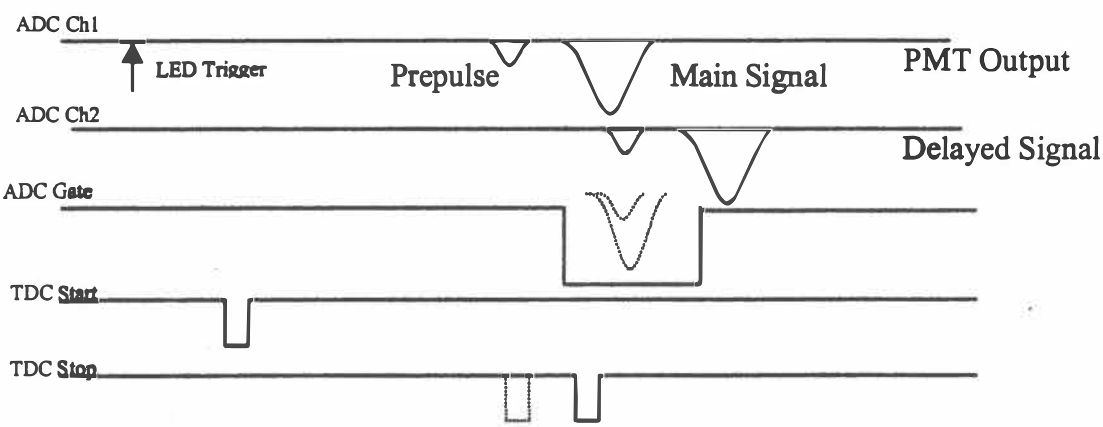

FIGURE 4.3: PREPULSE MEASUREMENT TIMING SCHEME

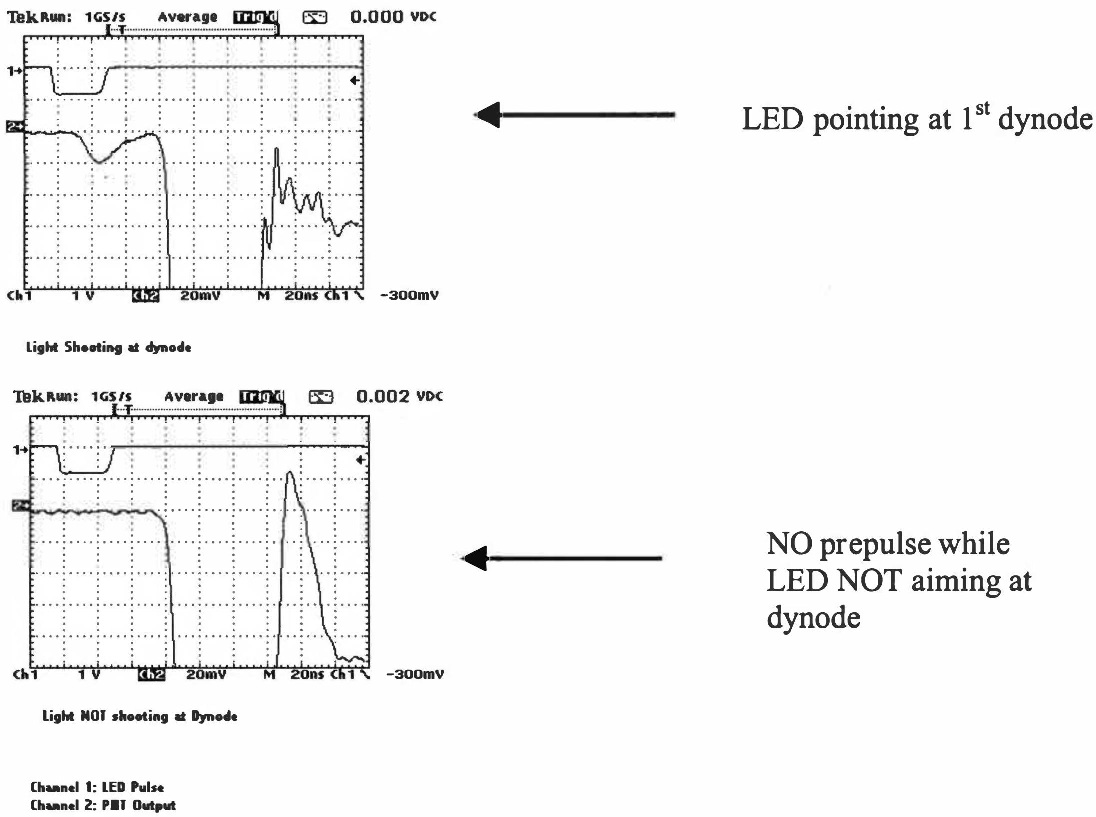

FIGURE 4.4: OSCILLOSCOPE SCREENSHOT - DIFFERENT INCIDENT LIGHT DIRECTIONS

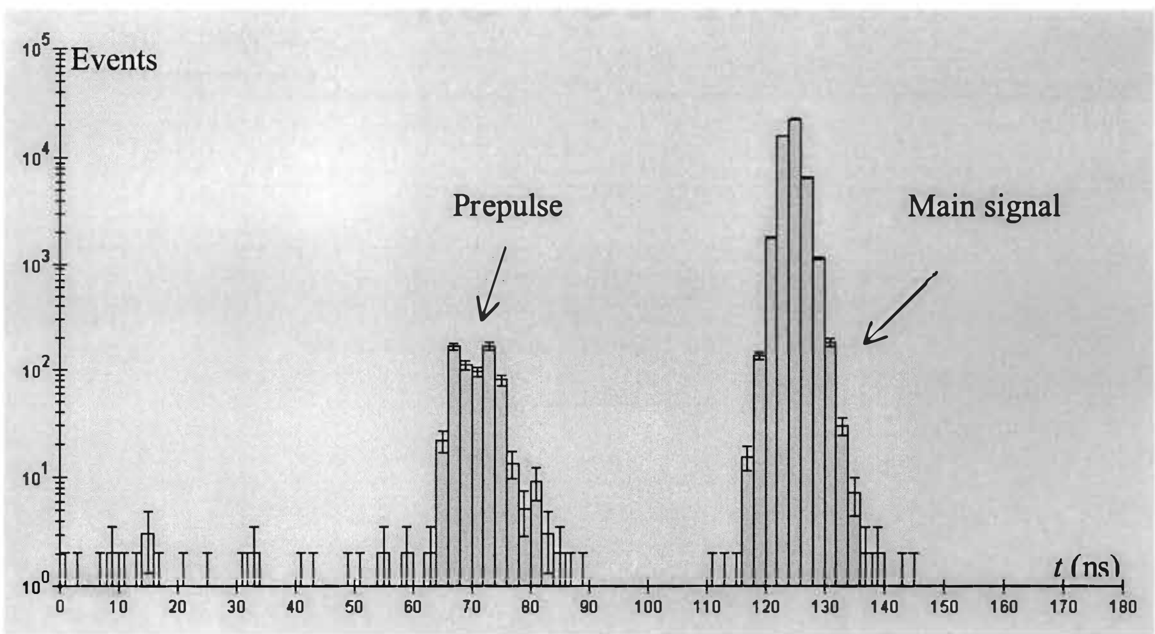

FIGURE 4.5: PREPULSE POSITION IN TIME SCALE

4.3.3 Prepulse amplitude property:

The amplitude distributions for prepulse and main pulse at different incident light intensities are shown in Figure 4.6. We fitted the amplitude distributions with the same function that we used in SPE measurement. For prepulse, the different gaussian peaks correspond to different number of dynode electrons after the first dynode. λ_d is the average dynode electron coming out from the first dynode. λ_c for main pulse is the average number of photoelectrons coming out from the photocathode.

4.4 Discussion

From the results presented above, we confirm the hypothesis for prepulse mechanism: Prepulse occurs around 60 ns before the main signal in R7250. The time difference corresponds to the drifting time of photoelectron. Prepulse was not observed when the incident light is not shooting at the first dynode and it has an order of magnitude less amplitude than main signal since it does not have amplification at the first dynode. All the results indicate that the prepulse is due to electron emission at the first dynode caused by incident photons.

- Consistency of cathode - dynode intensities

The position of the first peak and the width in prepulse spectrum fitting corresponds to the average value and fluctuation of amplification factor of the first dynode, which are the properties of the PMT and shouldn't depend on the incident light intensity. In other words, the fitted values for different incident light intensities should be consistent. The average value for the first peak position is 5.95±0.17 channels (0.25pc / channel) away from the pedestal. The average width for the first peak is 3.03±0.17 channels.

- Linearity of first dynode

Since the dynode efficiency is fixed at a given wavelength, the average number of dynode electrons (λ_d) is proportional to the incident light intensities, which is represented by the average number of photoelectrons (λ_c). From figure 4.7 we can see that they have pretty good linearity.

- Gain at first dynode

Since the prepulse and main signals represent basically the same mechanism, they should have similar amplitude distribution distributed by Poisson Law. The reason that prepulse is smaller than the main pulse is because it doesn't have the amplification at the first dynode.

Pulse Height Distribution - Prepulse Vs Main pulse

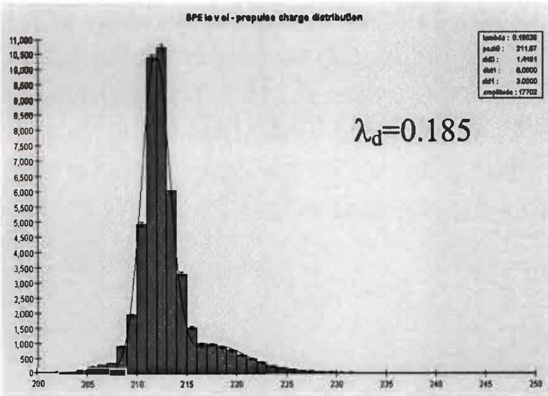

Prepulse 1.6 P.E.

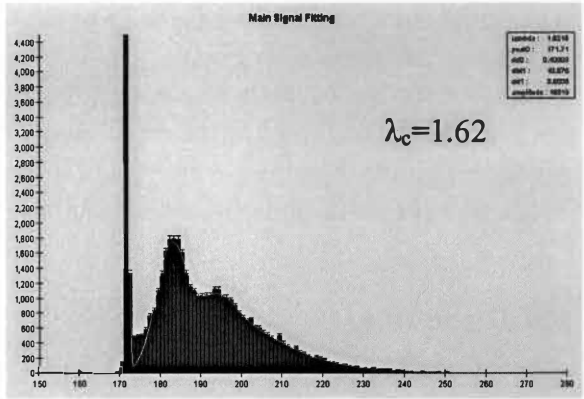

Main Pulse 1.6 P.E.

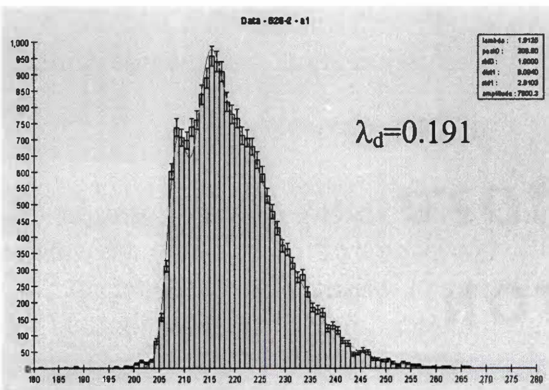

Prepulse 16 P.E.

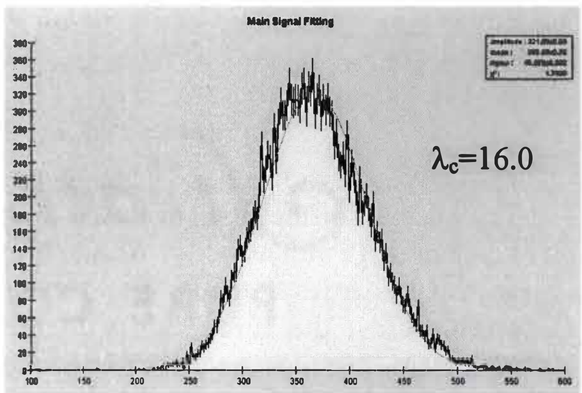

Main Pulse 16 P.E.

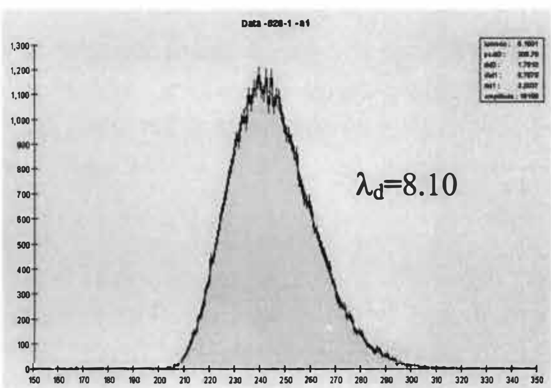

Prepulse 54.9 P.E.

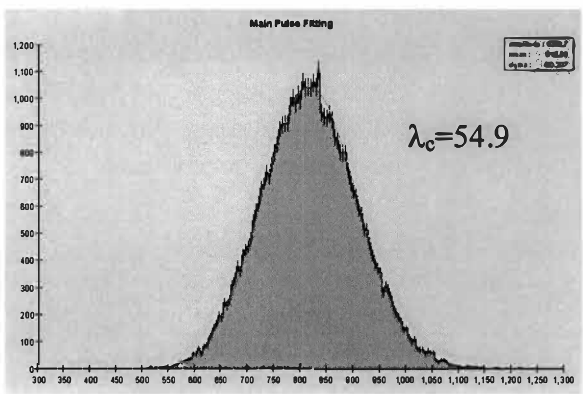

Main Pulse 54.9 P.E.

FIGURE 4.6: PULSE HEIGHT DISTRIBUTION FOR PREPULSE AND MAIN PULSE AT DIFFERENT LIGHT INTENSITIES

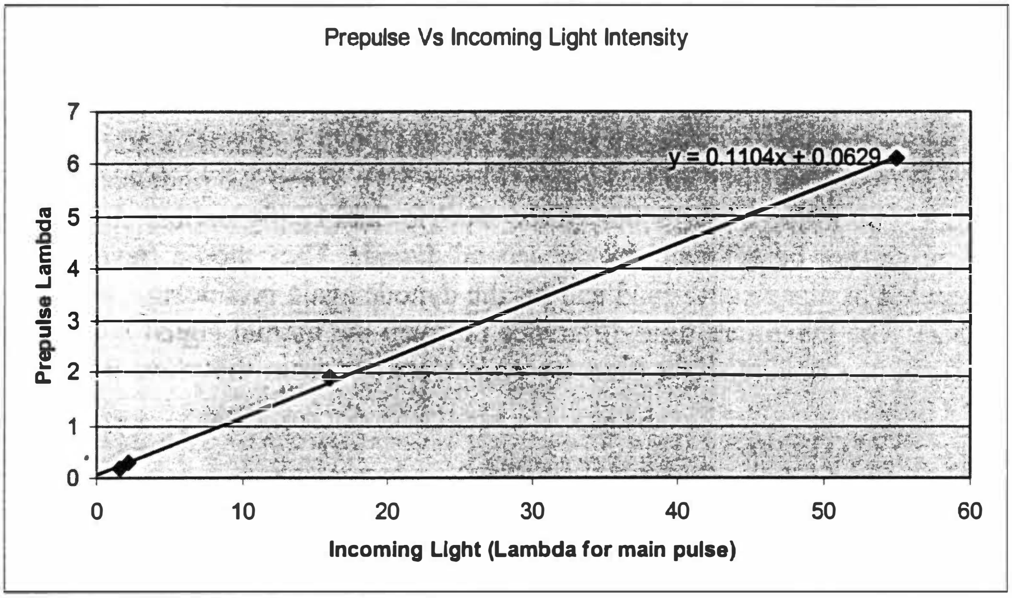

FIGURE 4.7: PREPULSE SIGNAL VS INCIDENT LIGHT Intensities

By comparing the amplitude spectrum of prepulses and that of main pulses, we can determine the gain at the first dynode. Since the position of first peak in the main pulse amplitude spectrum corresponds to SPE while in prepulse spectrum it corresponds to SDE (Single Dynode Electron). The ratio of the main pulse first peak position to the prepulse first peak position provides the gain at the first dynode:

$$G_1 = 102 / 5.95 = 17.1$$

- Photocathode Efficiency

The photocathode efficiency is defined as the number of dynode electrons emitted from the dynode divided by the number of incoming photons. The Quantum Efficiency of the photocathode at wavelength 400nm is 22%. From the discussion in §4.1 we have:

$$\frac{\lambda_c}{\lambda_d} = \frac{N\xi}{N(1-\xi)\eta} = \frac{\xi}{(1-\xi)\eta}$$

$$\eta = \frac{\lambda_d \xi}{\lambda_c (1-\xi)} = \frac{0.1104 \times 0.22}{1-0.22} = 3.1\%$$

Chapter V Afterpulse Measurements

Another type of abnormal response that R7250 PMT will generate is afterpulse, which will come up to 120ns after normal pulse (Figure 5.1). When the photoelectron hits the first dynode, due to the imperfection of the electric field configuration, some secondary electrons might not be collected by the second dynode. They would travel back in the tube, be pulled by the electric field and hit the dynode again producing a delayed signal (Figure 5.2). The maximum time difference between the normal signal and the delayed signal will be the double flight time for photoelectrons from the photocathode to first dynode.

In this section, the time spectrum measurement of delayed signal is described. Two afterpulse types are discussed: one with the main signal presented is due to partial collection of secondary electrons at the dynode (Induced Afterpulse), while the other type is due to back scattering of incoming photoelectrons (Delayed Main Pulse). The amplitude measurement shows that both types of afterpulses are Single Photo Electrons.

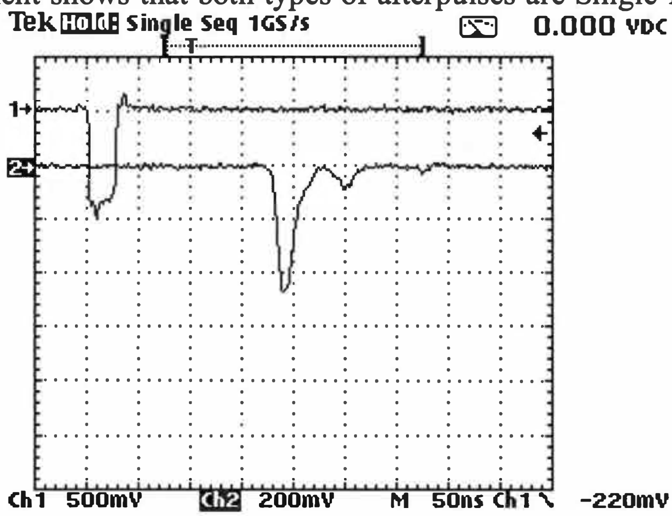

FIGURE 5.1: TYPICAL AFTERPULSE FOR R7250

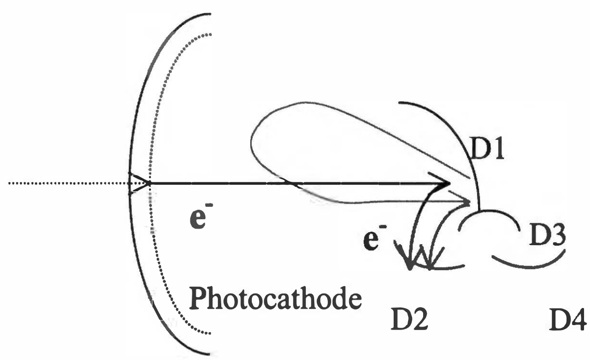

FIGURE 5.2: AFTERPULSE MECHANISM

The probability of occurrence for Induced Afterpulse was calculated to be 3.5% and 4.4% for Delayed Main Pulses.

5.1 Afterpulse Mechanism

When photoelectrons come to the first dynode with the energy around 800 eV, they will knock out a number of electrons (17 electrons according to our measurement). Since the electric field configuration is not perfect, some of the secondary electrons will not be colleted by the second dynode depending on the initial velocity and energy. Also some photoelectrons will have a small probability to be scattered back without producing any secondary electrons. The time delay for afterpulse is the total flight time for those electrons that are not collected by the second dynode. By analyzing the coincidence of the main signal and the delayed signal, we can separate the two types of afterpulses and study them separately.

5.2 Experiment Setup

In order to analyze the afterpulses, we need to catch both main signal and delayed signal at the same time. In our measurement we used a delayed PMT output to fit into the same ADC gate and then a delayed discriminator output to catch both signals in TDC. The experiment setup is shown in Figure 5.3.

By carefully selecting the start signal position, we can catch both the main signal and the delayed signal in two different channels of a single hit TDC (LeCroy 2228A). The start signal is chosen at right after the main signal falls under the threshold, the ADC gate is chosen to catch both signals, and the threshold is set at 20mV to catch most of signal. The timing scheme is shown in figure 5.4.

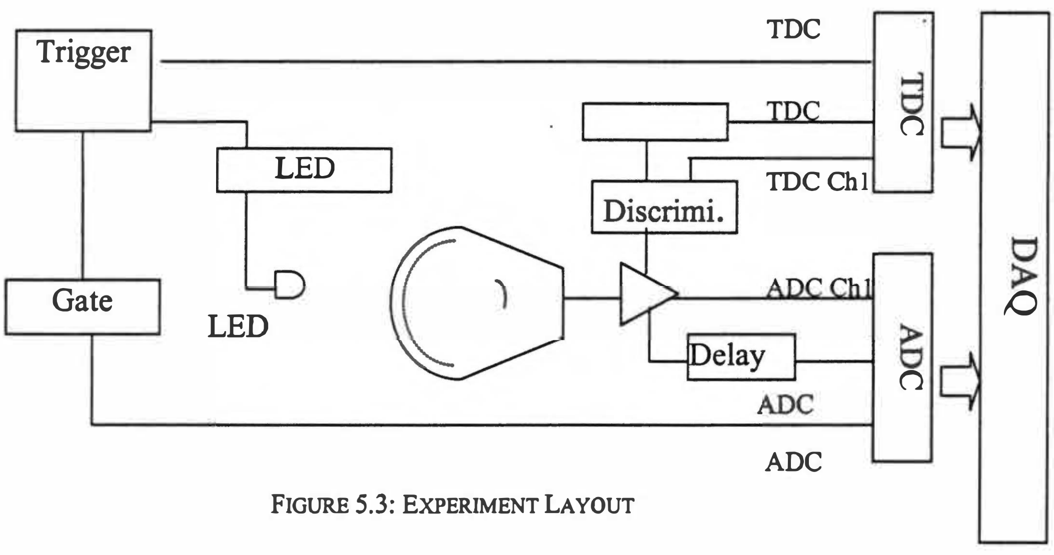

FIGURE 5.3: EXPERIMENT LAYOUT

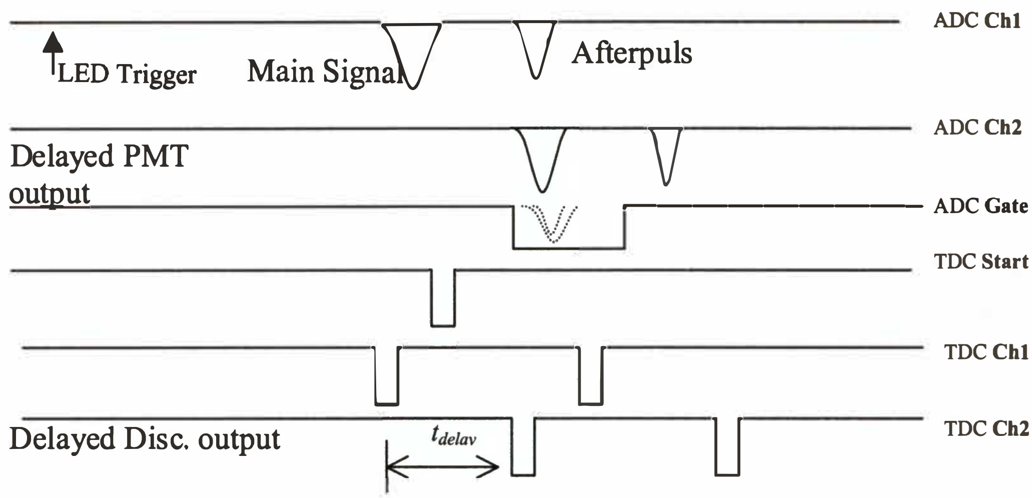

FIGURE 5.4: AFTERPULSE MEASUREMENT TIMING SCHEME

5.3 Experimental Results

- Time spectrums

From the layout above, we can see that the first TDC channel will catch the main signal, while the second channel will catch the delayed signal in a time window of 200ns. The time distribution for the delayed pulses is shown in Figure 5.5:

The delayed pulses consist of two types afterpulses as shown in Figure 5.6: those that have a normal main signal prior to the delayed signal, and the ones that do not have a normal signal present at the main signal position in time scale.

The difference between two spectrums suggests that there are two different types of afterpulses. For the afterpulses that have main signal presented, the time difference spectrum between the main signal and delayed afterpulses is plotted in figure 5.7. The front edge of time spectrum is due to the discriminator when the afterpulse gets too close to the main pulse and it becomes impossible to resolve. There might be some afterpulses that are hidden inside the main SPE pulse. This might lead to some deviation from the Poisson distribution in main signal spectrum.

- Amplitude spectrum

The afterpulse amplitude spectrum is shown in Figure 5.8. By comparing the spectrum with the SPE spectrum, we can see that the afterpulses have same amplitude distribution as SPE's.

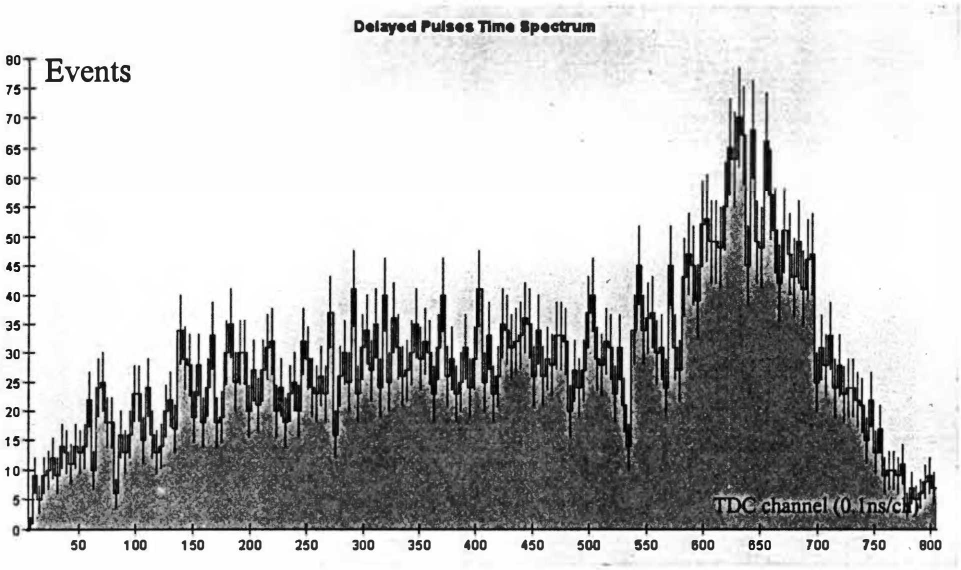

FIGURE 5.5: DELAYED PULSES TIME DISTRIBUTION

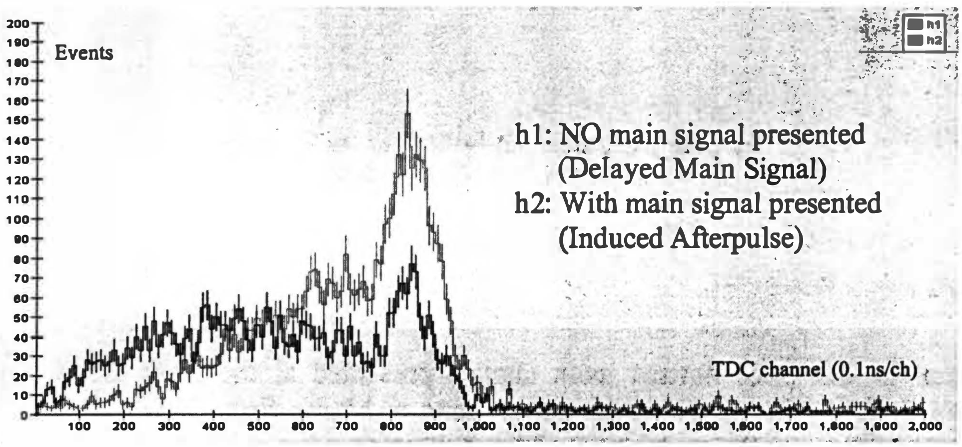

FIGURE 5.6:TWO TYPES OF AFTERPULSES

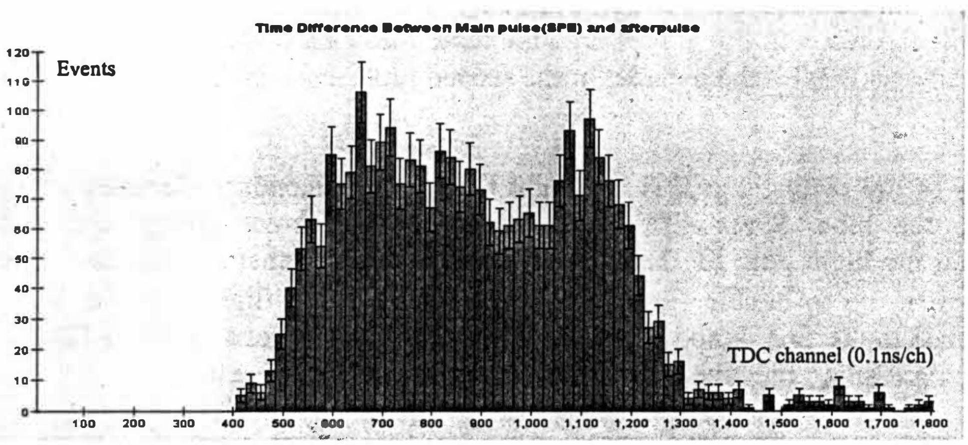

FIGURE 5.7: TIME DELAY BETWEEN MAIN PULSE AND AFTERPULSE

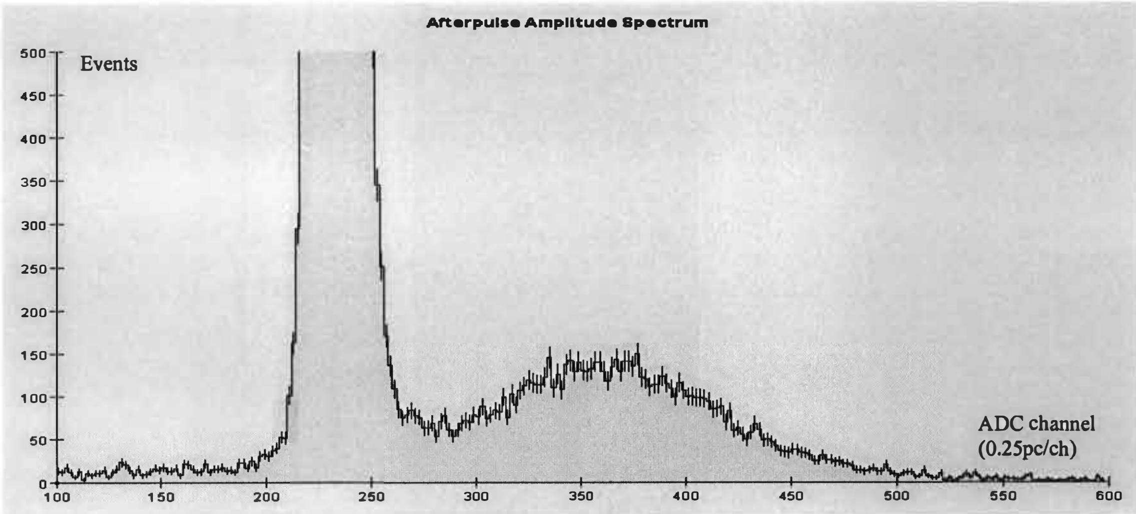

FIGURE 5.8: AFTERPULSE AMPLITUDE DISTRIBUTION

5.4 Discussion

The data above indicates that there are two types of afterpulses: one with normal main signal presented before the delayed pulses and one without any "main" signal presented. We should treat them separately, as follows in the next subsections:

5.4.1: Induced Afterpulse

The afterpulses that have normal main signals presented at the front are defined as *Induced Afterpulse.* When a photoelectron coming to hit the first dynode, it will knock out a number of secondary electrons. The collection efficiency of these secondary electrons depends on the particular electric field configuration. Some of them are collected by the second dynode and amplified by the electron multiplier forming the main pulse, while the rest will travel back into the tube. These electrons will be pulled by the electric field and will hit the dynode for the second time hence giving a delayed signal in the output of PMT.

The delay of the second signal is the flight time of the secondary electron(s) traveling back into the tube. Since different electrons have different energy and different trajectories, the flight time for them are different with each other and the time spectrum will be spread up to double flight time 2τ, where τ is the flight time for SPE from photocathode to the first dynode. The spectrum detail will depend on many factors such as electric field inside the tube, the work function for the dynode, etc.

After normalization and double electron correction, we calculated the probability of occurrence for *induced afterpulse* as 3.5% per single photoelectron.

5.4.2 Delayed Main Pulse

The other type of afterpulse does not have the presence of the main signal. Strictly saying, we should define it as "Delayed Main Signal" since they are actually the main pulses delayed due to back scattering.

When photoelectrons are coming to the dynode, there is a small probability that they might be scattered back to the tube without knocking out any secondary electrons. If the collision is elastic, the energy of the photoelectron will be conserved. Most of the scattered electrons will travel all the way back to the photocathode and be pulled by the field back to the dynode. The total time of flight will be 2τ (~120ns). Thus, it will form a peak around 120ns in time spectrum of delayed main pulse.

As in the induced afterpulse case, we calculated the probability of occurrence for delayed main pulse and it is of 4.4% per single photoelectron.

5.4.3 Secondary effect of afterpulse

From the previous discussion, an afterpulse should be able to produce another secondary afterpulse with some small probability. Those pulses should be further delayed in time scale. We observed this secondary effect in our latepulse measurement with a multi-hit TDC (Chapter VI). A typical time spectrum with large incident light intensity is shown in Figure 5.9.

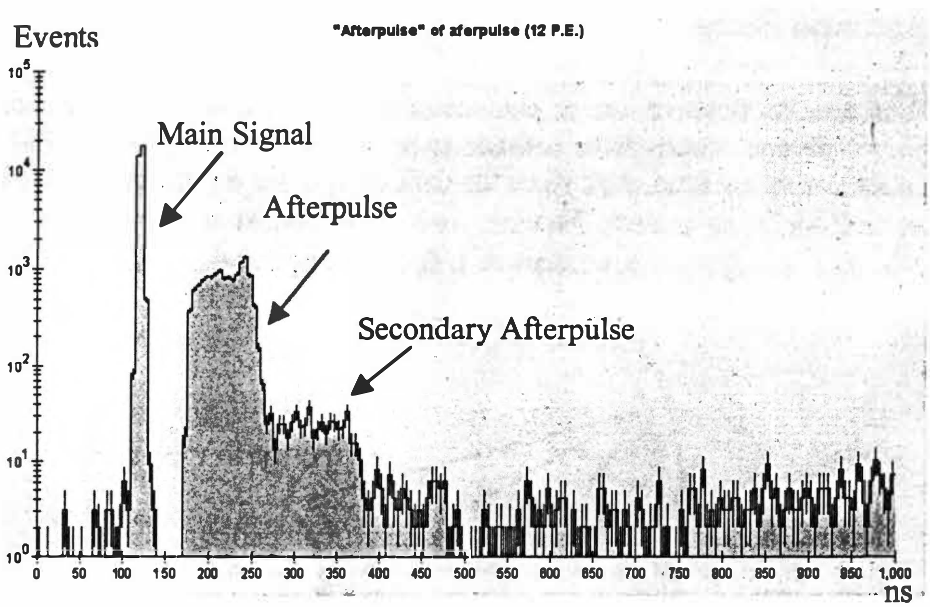

FIGURE 5.9: SECONDARY EFFECT OF AFTERPULSE

Chapter VI Late Pulse Measurements

Another kind of abnormal pulses for PMT R7250 is latepulse - sometimes there are some delayed pulses microseconds after the main pulse, which are also referred as "afterpulse" in many cases. The main origin of these pulses is due to the ionization of the residual gases inside the tube [8][9]. The mechanism of laterpulse is shown in Figure 6.1. When photoelectrons are coming from the photocathode to the dynodes, they might ionize the molecules of the residual gas, at the same time, an additional electron is produced. The positive ions will drift to the photocathode due to the electric field and knock out photoelectrons; they travel to the dynode producing a late pulse. Since the ions are much heavier than electron, the delay is in the order of microseconds. The exact delay time depends on the type of the ions and the electric field configuration.

In this section we will describe the measurement for late pulses time spectrum and amplitude spectrum. Two incident light intensities were used in our measurement below: SPE level and 12 P.E. level. A multi-hit TDC was used to catch all the pulses after the main signal. By comparing the result with the Hamamatsu measurement, we can see that multi-hit TDC provides more detailed information about late pulses. In addition, we tried to map out the different peaks in time spectrum with different types of ions. The amplitude measurement suggested that they are all single photoelectrons. The total probability of occurrence is calculated to be 9%.

6.1 Experiment Setup

The drifting time for positive ions to photocathode is in the order of microseconds, so the flight time of photoelectrons from cathode to dynode and time spread of PMT electron amplification can be ignored. And since the dark current for our measurement is at 30khz level, the average time interval between two noise pulses will be 30μs. In order to measure the time spectrum in a window of 100μs, we applied the LeCroy 4208 as a

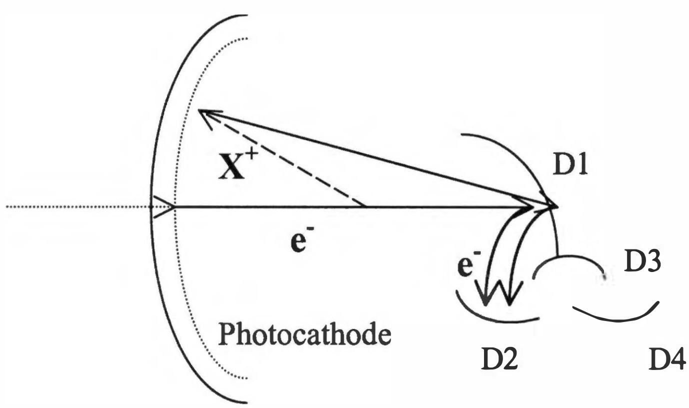

FIGURE 6.1: LATEPULSE MECHANISM

multi-hit TDC in our measurement; it can catch up to 6 pulses including the main signals. This long-range multi-hit TDC can record all the hits during the time interval of 100μs after the main signal.

If the photoelectrons are independent during the ionization, the total late pulse signal will be proportional to the incident light. To check the consistency, we applied two light intensities below: SPE level and 12 P.E. Since the background (dark current) is constant during all the measurement, we should see a much more detailed structure in time spectrum with high light intensity. The experiment setup is shown in Figure 6.2:

To measure the amplitude, we used the output signal from the PMT itself as the trigger for the ADC gate. By carefully selecting the delay of the PMT signal we can catch the output pulse in the ADC gate that is triggered by the signal itself. To control the region in which the pulse amplitude is measured, we used another gate generator to generate the "veto" signal for ADC gate. The whole timing scheme is shown in Figure 6.3.

6.2 Late Pulses Results

6.2.1 Time spectrum

Since the dark current rate is 30Khz in our measurement and its level is constant, the accuracy of background subtraction will directly affect the experimental results, especially for low light intensity. Thus, we applied a background measurement for latepulses to obtain a better background subtraction.

As for SPE level light signal, the late pulse events are very few compared to the background noise. These signals are buried in the noise signal. Figure 6.4 shows the time spectrum of latepulses in the time interval 0-60 microseconds after the main pulses

The first bin is the main signal and there are some latepulses events that can be seen up to 25 microseconds. The latepulses events are too few to form a detailed structure. After subtracting the background by using the background measurement, the probability for latepulse is calculated to be 11% per single photoelectron.

To measure the detailed structure of latepulses we increased the incident light intensity to 12 P.E. The background is the same but the latepulses signals would be 12 times more frequent if the photoelectrons are independent with each other. The time spectrum is shown in Figure 6.5.

Better structure can be seen from this spectrum: a huge peak can be observed at the position 17μs. Another peak is sitting at 4.4μs while a small sharp peak is overlapped at 2.5μs.

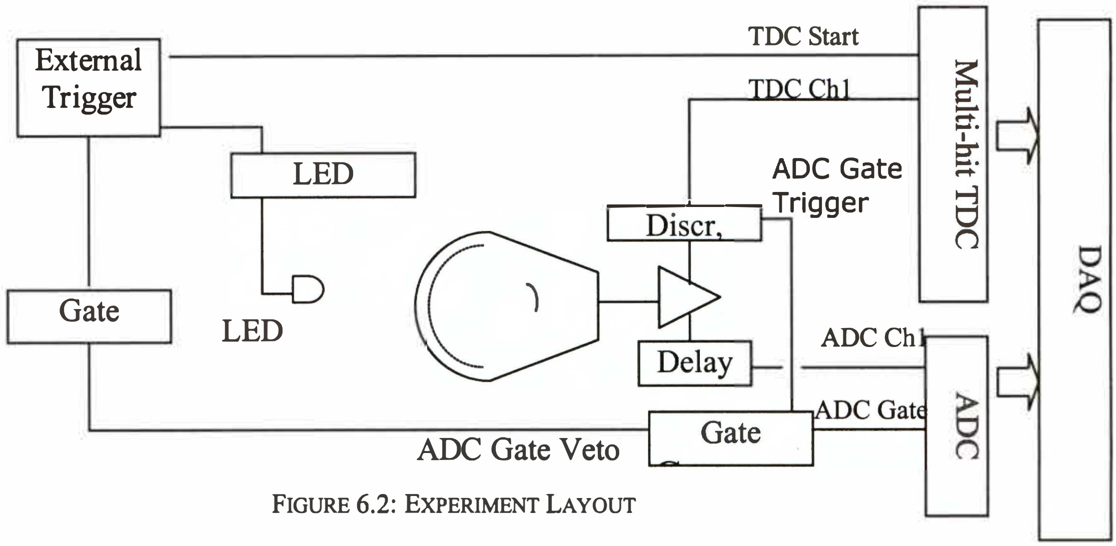

FIGURE 6.2: EXPERIMENT LAYOUT

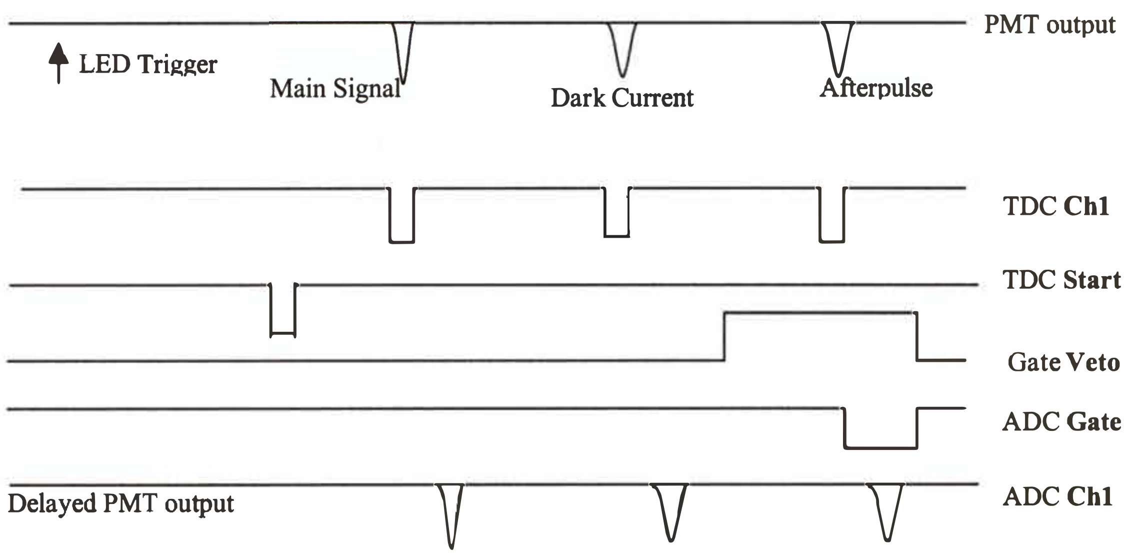

FIGURE 6.3: LATEPULSE MEASUREMENTS

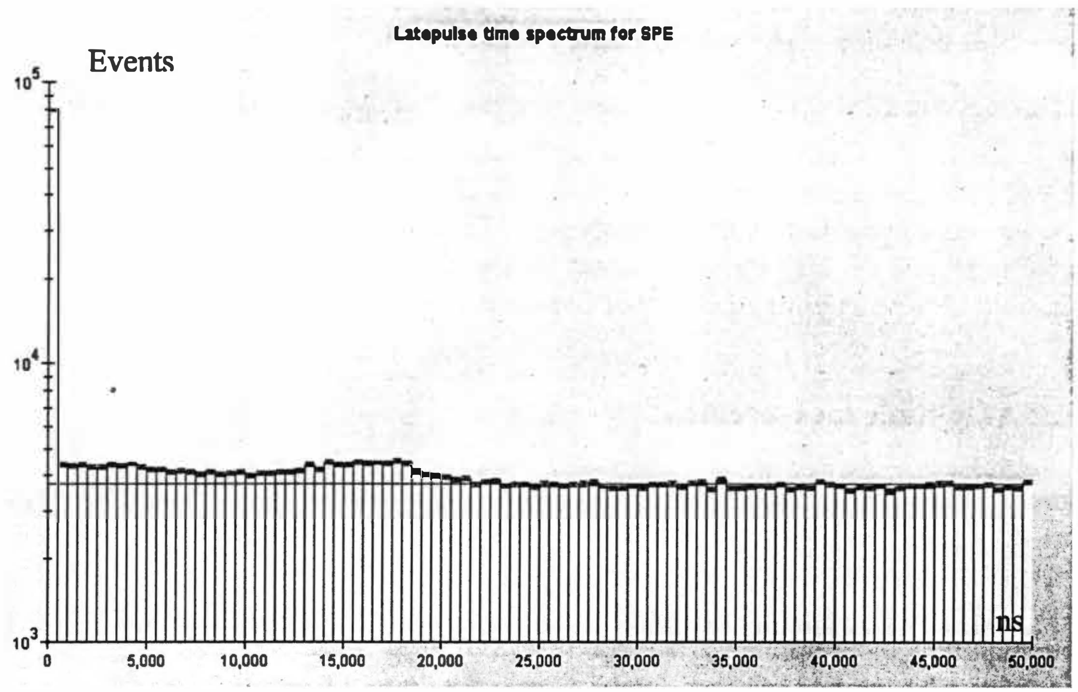

FIGURE 6.4: LATEPULSE TIME SPECTRUM (LOW LIGHT INTENSITY)

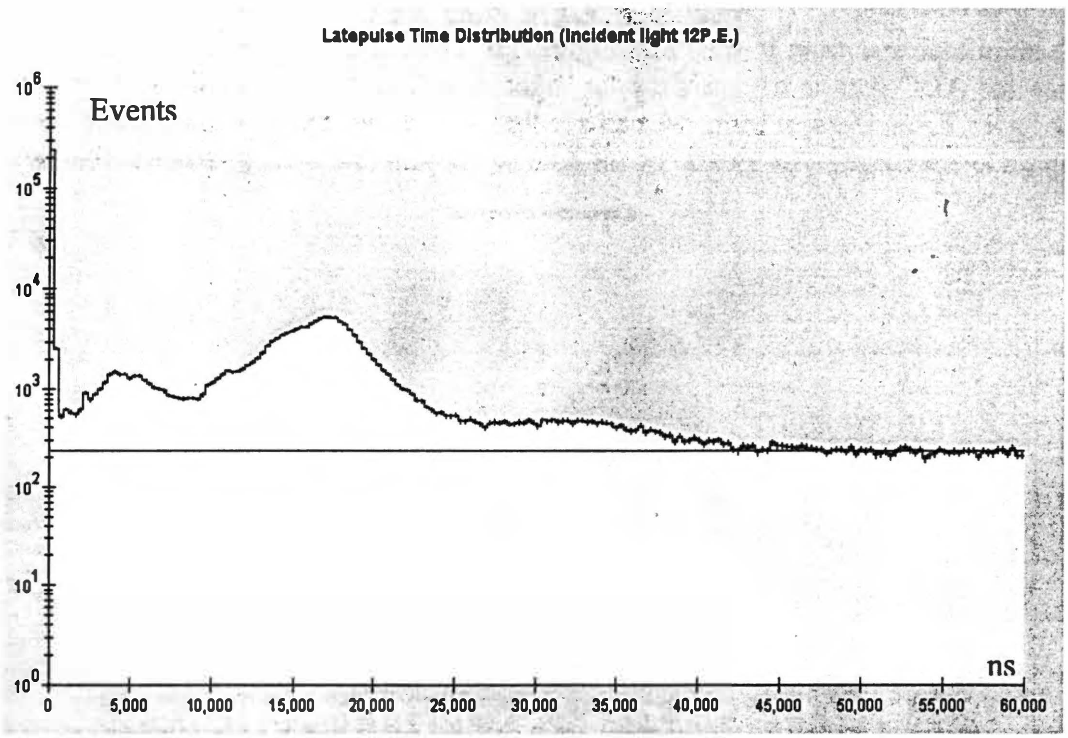

FIGURE 6.5: LATEPULSE TIME SPECTRUM AT LARGE LIGHT INTENSITY

The broad peak at 30μs was not seen in the pervious spectrum due to the relatively low statistics. After subtracting the background from the spectrum, the probability for latepulse is calculated to be 9% per single photoelectron.

Comparing the probability of occurrence in our two measurements, the 2% difference is due to the discriminator cutoff for low light intensities. Since the discriminator is set at 25% of SPE amplitude spectrum, it will cut off 25% of latepulses (and dark current) and 25% for main signal if the light intensity is at SPE level. For high light intensity the main signal is around 12 P.E. that has almost no cutoff due to the discriminator. Thus, we measured 25% probability of that in SPE measurement.

6.2.2 Amplitude measurement

Since different peaks in time spectrum assumingly correspond to the different types of ions in the PMT, we measured the amplitude spectrum for latepulses (with dark current) at the several peak positions.

The amplitude measurement is done at delays of 40μs (pure dark current), 17μs, 4.4μs and 2.2μs. The capture window for ADC gate for 40μs, 17μs and 4.4μs peaks was 1μs and for 2.2μs peak was 500ns because of the sharpness of the peak.

The amplitude spectrum is shown in Figure 6.6. The pedestal position is at channel 300. Since the ADC gate is triggered by the signal itself, there is no pedestal caught in the ADC gate. From the spectrum, we can see that all the four measurements have the same amplitude spectrum. The peaks of all four spectrums are sitting around channel 400

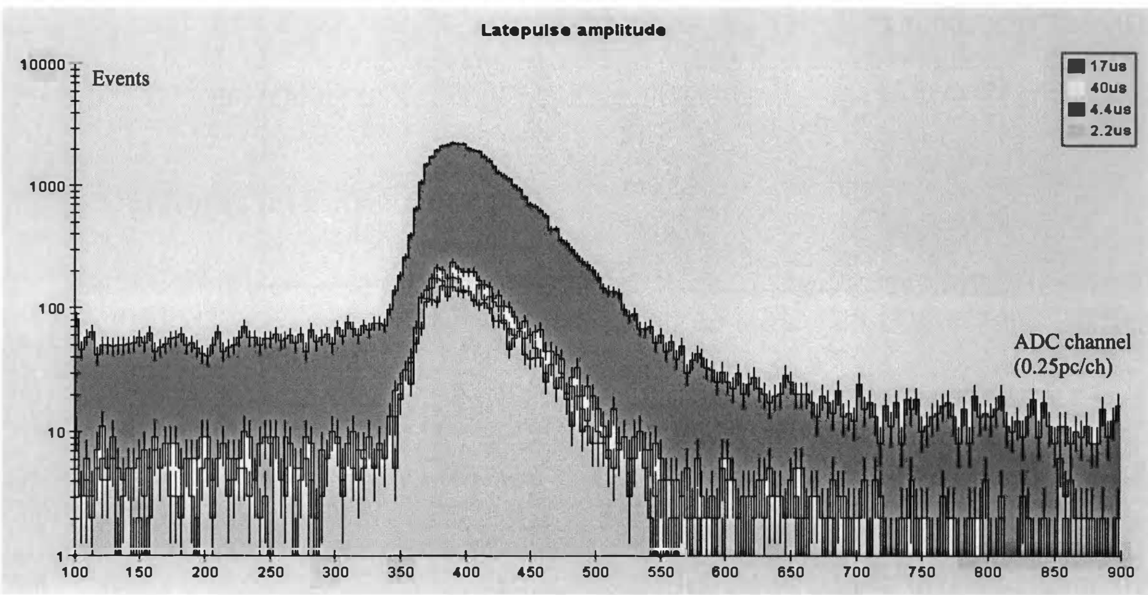

FIGURE 6.6: LATEPULSE AMPLITUDE DISTRIBUTION AT 4 PEAKS

(~100 channels above the pedestal). These results suggest that all the four spectrums are from single photoelectrons.

6.3 Discussion

6.3.1 Single-hit Vs Multi-hit TDC

Late pulse spectrum measurement was also made by Hamamatsu. The result is shown in Figure 6.7. The time spectrum is measured by a single hit TDC and a window of 33.4μs was measured. By comparing our results and the Hamamatsu measurement we noticed:

- Similar structure

  We can see two peaks from the Hamamatsu measurement and both of them can be seen in our measurement. The shoulder of the 17μs peak can be seen in both spectra.

- Detailed structure in multi-hit spectrum

  There are several structures that are not seen in the spectrum provided by Hamamatsu: The small peak around 2.2μs is not seen because of the distortion of single hit TDC. The broad peak after 30μs is not seen since the measurement range and signal statistics for single hit TDC is limited by the dark current.

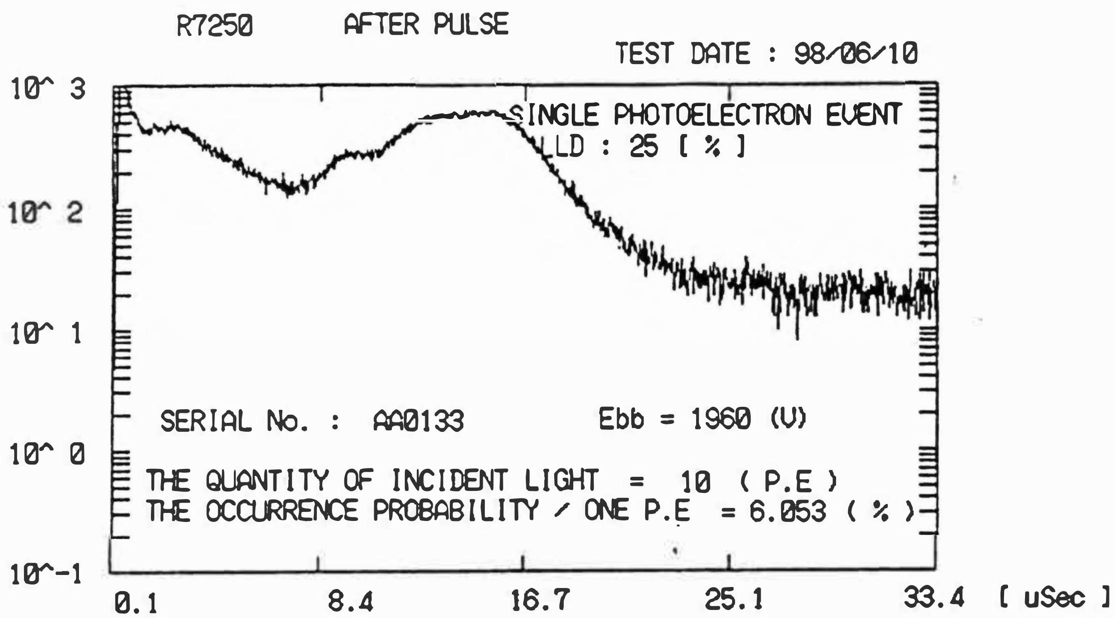

FIGURE 6.7: HAMAMATSU LATEPULSE MEASUREMENT

Since the Hamamatsu measurement used a single hit TDC it can only catch the first hit after the main signal. If the signal were uniformly distributed (dark current), the time spectrum in single-hit TDC would be exponential. The late pulses spectrum is distorted and cannot be used in precise study of latepulses.

From the discussion above, we can also see that it is very difficult to precisely determine the background level. The number of latepulses needs correction as well, since one main signal may be followed by several latepulses. It is hard to accurately calculate the afterpulse probability of occurrence. In order to study the latepulse in detail and precisely measure the probability of occurrence, the multi-hit TDC has to be used to replace the single hit TDC.

6.3.2 Origin of latepulses

Since the main reason for latepulses is the ionization of residual gases inside the PMT, it is possible to use PMT as a spectrometer to map out the residual gas molecules [9]. From the time spectrum of latepulses three peaks are observed around 2.2μs, 4.4μs and 17μs, which might be due to the presence of the noble gas molecules inside the tube.

Since the time delay is the drifting time for positive ions to photocathode, it should depend on the type of ions (mass charge ratio) [9], electric field configuration and the point of origin. If two ions are generated at the same point and follow the same path to the photocathode, the drifting time should be proportional to the square root of mass charge ratio. Exact identification of ions is difficult since electric field needs to be known [8].

The point of ionization depends on type of the residual gas molecule and their electron cross-section (The cross-section curve for *He* against energy is shown in Figure 6.8 as an example). The operating voltage between the photocathode and first dynode is around 815V. We can see that for *He* the electron has a maximum cross-section around 100eV, this means that most of helium molecules inside the tube will be ionized in the middle of the tube. Again, in order to calculate the exact time distribution we need the electric field configuration and the cross-section for the particular type of molecules.

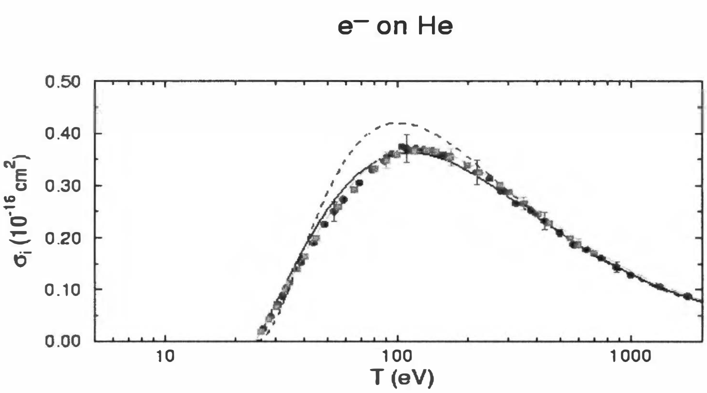

Figure 6.8: *He* ionization cross-section [10]

If we approximate the field inside the tube as a spherical field ($1/r^2$), which is quite rough for R7250, we can calculate the drifting time for different ions starting from different original point. The result is shown in Table 6.1. By comparing the calculated value, especially in the middle range (7cm – 21cm), and the peak position in time spectrum we can identify several possible types of ions that might be responsible for our time spectrum:

- Hydrogen for peak at 2.2 microsecond (1.6μs – 2.6μs in our calculation)
- Helium for peak at 4.4 microsecond (3.2μs -5.2μs in our calculation)
- Argon for peak at 17 microsecond (14μs – 24μs in our calculation)

The broad peak at 33μs was not identified. From the discussion above we should remember the exact identification of ions depends on many critical factors so it is difficult to find out the exact origin of the latepulses.

Table 6.1: Drifting Time for Different Ions

Orig. Pos.	H+	H2+	He+	N2+	O2+	Ne+	Ar+	Xe+
3cm	0.999	1.413	1.998	5.286	5.651	4.468	9.156	11.434
5cm	1.335	1.888	2.67	7.064	7.551	5.97	12.234	15.278
7cm	1.614	2.283	3.228	8.541	9.131	7.219	14.794	18.475
9cm	1.853	2.621	3.706	9.805	10.482	8.287	16.983	21.209
11cm	2.058	2.91	4.116	10.89	11.642	9.204	18.862	23.555
13cm	2.232	3.156	4.464	11.81	12.626	9.981	20.456	25.545
15cm	2.376	3.36	4.751	12.571	13.439	10.624	21.774	27.191
17cm	2.489	3.52	4.978	13.171	14.081	11.132	22.813	28.489
19cm	2.571	3.636	5.142	13.605	14.545	11.499	23.565	29.428
21cm	2.62	3.705	5.239	13.862	14.819	11.716	24.01	29.984

Chapter VII Summary

In order to have input for KamLAND detector simulation, we studied the Hamamatsu R7250 photomultiplier tube's response to the single photoelectron and all types of abnormal pulses it might produce. The results of our measurements show that:

(I) PMT response to Single Photoelectron:
Single Photoelectron pulse height distribution is measured. By measuring the gain at the first dynode in R7250, the contributions in the SPE spectrum width is better understood. The electron multiplier has ~27% fluctuation while addtional 20% fluctuation should be due to other effect such as non-uniformity of collection efficiency, etc.

(II) Prepulse:
The result of the measurement confirmed the prepulse mechanism. We introduced the technique to measure the efficiency to photons and the secondary emission ratio for the first dynode, which can be used to calculate the contribution of dynode system in SPE pulse height distribution. The secondary emission ratio at the first dynode is measured to be 17.1 at operating voltage 1960V. The dynode efficiency is measured to be 3.1%.

(III) Afterpulse:
By studying the coincidence of afterpulse and normal PMT signal, we discovered two types of afterpulses: "induced afterpulse" and "delayed main signal". They have different mechanism and time spectra measured for both types. The amplitude measurements indicate that they are both single electrons in spectra and the probability of occurrence is 3.5% and 4.4%.

(IV) Latepulse:
A multi-hit TDC is introduced in our latepulse measurement. In comparison with Hamamatsu latepulse measurement, we measured more detailed time spectrum for R7250 with a better subtraction of the background. The total probability of occurrence of laterpulses is 9%. The results of amplitude measurements indicate that they are all single electrons in spectra.

These PMT measurements will provide a more accurate input for the Monte Carlo simulation in KamLAND experiment. Thus they will result in better data analysis hence more precise physics result.

[1] Karsten M. Heeger, *"Resolving the solar neutrino problem",* Europhysics News (2001) Vol. 32 No. 5
[2] D.E.Groom *et al.*, *"Review of Particle Physics,"* The European Physical Journal C15, 1-878 (2000).
[3] P.Alivisatos *et al.*, *"KamLAND: A liquid scintillator anti-neutrino detector at the Kamioka site,"* STANFORD-HEP-98-03, Tohoku-RCNS-98-15 (1998)
[4] T.Kajita, "*Status of Super –Kamiokande and the JHF Kamioka neutrino project",* Super Kamiokande collaboration and JHF-SK neutrino WG, Beyond02, Oulu, (2002)
[5] Tajashira Kenji, *"Study of 17" Photomultiplier"*, Master Thesis, Tohoku University, Japan
[6] Hamamatsu catalog, *"Photomultiplier Tubes and Assemblies for Scintillation Counting and High Energy Physics"*, Hamamatsu Photonics K.K. (1998)
[7] Hamamatsu R7250 Tube Passport, Hamamatsu Photonics K.K.
[8] G.A.Morton, H.M.Smith and R. Wasserman, IEEE Trans. Nucl. Sci. NS-14, 443 (1967)
[9] P.B.Coates, *"The origins of afterpulses in photomultipliers"*, J.Phys. D: App. Phys., Vol. 6, (1973)
[10] National Institute of Standards and Technology, *"Electron Impact Cross Section Database"* (2001)

Vita

Wei Jiang was born in Beijing, P.R.China on May 17, 1977. After graduate from The High School Attached to the People's University, Beijing in 1994, he entered Peking University in Beijing, China and four years later he received a Bachelor Degree in Electronics with a major in Electronics and Information Systems in July, 1998. He attended The University of Tennessee, Knoxville in 1999 and received M.S. Degree in Physics in August, 2002. His research interests include neutrino oscillation, ultra cold neutrons and neutron-anti neutron oscillation.

5176 3768 4
09/24/02 MAB